DOCTORAL THESIS

Experimental and simulation studies on crystal growth and crystallinity evaluation of organic materials and polymers

Xiaoran Yang

Materials Chemistry and Engineering Course

Graduate School of Chemical Sciences and Engineering

Hokkaido University

(Doctoral Supervisor: Toshihiro SHIMADA, Professor)

COTENTS

Chapter 1

General Introduction

1.1 Functional materials

Functional materials refer to materials that have specific functions through the treatment of light, electricity, magnetism, heat, chemistry, biochemistry, etc[1-9]. Functional materials cover a wide range of fields, specifically including optical functions, electricity functions, magnetic functions, separation functions, shape memory functions, and so on. Functional materials are found in all classes of materials, typical functional materials, for example, practical superconducting materials represented by NbTi [10,11] and Nb3Sn [12] have been commercialized and applied in many fields such as nuclear magnetic resonance imaging (NMRI), superconducting magnets and large-scale accelerator magnets; SQUID [13] is a model for the weak current application of superconductors. It has played an important role in the measurement of weak electromagnetic signals, and its sensitivity cannot be achieved by any other non-superconducting device. However, because the critical temperature of conventional low-temperature superconductors is too low, they must be used in expensive and complicated liquid helium (4.2K) systems, thus seriously limiting the development of low-temperature superconducting applications.

The emergence of high-temperature oxide superconductors has broken through the temperature barrier and raised the superconducting application temperature from liquid helium (4.2K) to liquid nitrogen (77K) [14,15]. Compared with liquid helium, liquid nitrogen is a very economical refrigerant and has a higher heat capacity which brings

great convenience to engineering applications. In addition, high temperature superconductors have a relatively high upper critical field which can be used to generate a strong magnetic field above 20T [16], which just overcomes the shortcomings of conventional low temperature superconductors. The research work of high temperature superconducting materials has made important progress in single crystal, thin film, bulk material and applications.

Energy materials such as solar cell materials are also a typical functional material, some reported solar cells even have a conversion efficiency as high as 40% [17,18]. Solid oxide fuel cells also got a lot of attention, such as solid electrolyte membranes and battery cathode materials, as well as organic proton exchange membranes for proton exchange membrane fuel cells, etc., which are all research hotspots.

Smart materials are the fourth-generation materials after natural materials, synthetic polymer materials, and artificially designed materials. Smart materials are one of the important directions for the development of modern high-tech new materials [19,20] that will support the development of future high-tech and realize structural functionalization and functional diversification. Scientists predict that the development and large-scale application of smart materials will lead to a major revolution in the development of material science [21]. Such as the British Aerospace Corporation uses wire sensors to test the strain and temperature conditions on the aircraft skin.; in piezoelectric materials, magneto strictive materials, and high conductivity The application of smart materials such as molecular materials, electrorheological fluids and magnetorheological fluids to drive

component materials in aviation has achieved many innovative results [22,23]. Functional materials are used in various fields because of they have many advantages, the market value and application value of functional materials are unparalleled.

1.2 Organic semiconductor

Since 1977 the first chemically doped polyacetylene [24] has been discovered which can be used as electrically active materials, organic semiconductors were beginning to attract people`s attention. In recent years, organic semiconductor-related technologies have developed rapidly [25-32], compared with traditional inorganic semiconductors, organic semiconductors have many advantages, one of the most important advantages is that the preparation process of organic semiconductors has relatively low requirements on conditions, such as high temperature [33], high vacuum deposition technology [34, 35] and photolithography [36] are not strictly necessary. Second, organic semiconductors can be obtained by chemical synthesis, inorganic semiconductors are based on silicon element, silicon is the second most abundant element on earth, but pure silicon is an intrinsic semiconductor and is non-conductive [37], n-type (p-type) semiconductors are fabricated by doping to improve the carrier mobility [38,39], now a days more and more high-performance semiconductor devices now require rare earth elements as dopants [40]. The cost of rare earth element mining is very high, so that the industrial cost is higher than that of organic synthesis.

Organic semiconductor materials can be dissolved in solvents and applied, which is

another advantage over inorganic semiconducting materials, such as applied on inkjet printing techniques [41]. As a newly developed device field, the performance improvement of organic semiconductors usually with the following process [42]: first the new synthesized organic semiconductor materials are applied to organic transistors, then through the thin film deposition process and liquid-phase process, find the best device structure and process method for the materials, finally test the materials properties through the device performance, choose a step to improve the material performance. At present, several organic materials with high mobility and widely used are reported, such as pentacene, 6,13-Bis(triisopropylsilylethynyl)pentacene (TIPS-pentacence), thiophene oligomers and C8-BTBT, etc [43-48].

The flexibility of organic semiconductors is better than inorganic semiconductors, organic semiconductor can adapt to different working environments to a certain extent and meet the deformation requirements of equipment. These devices rely on the compliant physical properties of organic polymers to maintain electrical continuity when deformed. Electrical connections within these devices are a point of weakness and have limited the types of materials and processes that can be used. Although inorganic semiconductors and metals have high conductivity, these materials will not commonly sustain repeated bending or stretching. A. Nathan et al. [49] show how metal can be added to components within flexible electronic devices, enabling conductivity to be maintained even after repeated deformation. Carbon nanotubes (CNT) and ZnO are currently more common flexible electronic device materials [50,51], Carbon nanotubes are promising materials

for flexible electronics due to their higher intrinsic carrier mobility and mechanical flexibility, Zinc oxide is a kind of wide band gap semiconductor material.

Although organic semiconductors have many advantages, they cannot completely replace inorganic semiconductors. The mobility of organic semiconductor materials can reach 20-40 $cm^2/(V \cdot s)$, or even 100 $cm^2/(V \cdot s)$ [52-54], but it is still far from inorganic semiconductors, as well as the on/off ratio and threshold voltage. Nonetheless, organic semiconductors have applications in sensors, wearable devices, and curved screens due to their low cost and high flexibility. Figure 1-1 shows the flexible organic field-effect transistor (picture from Wikipedia) and organic optical sensor (Someya Laboratory, University of Tokyo).

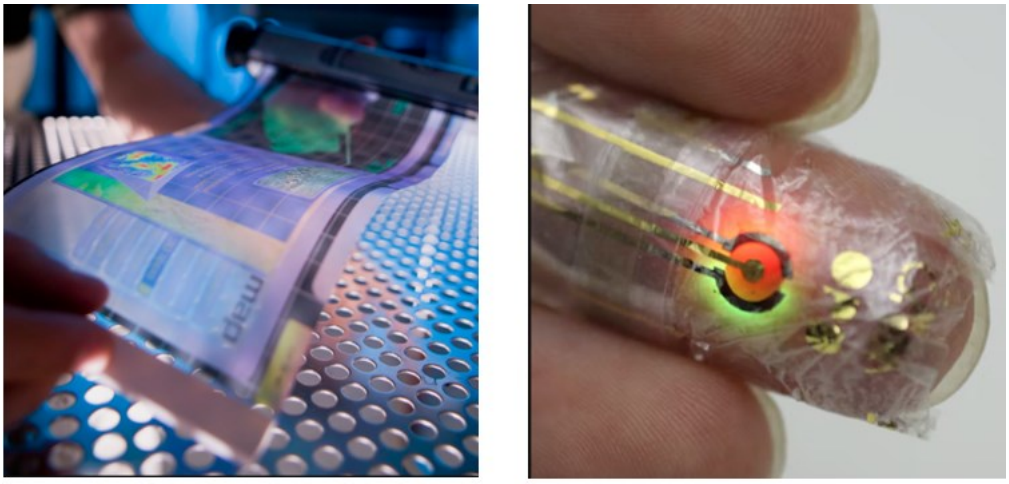

Figure 1-1 Flexible organic devices.

1.3 Molecular dynamics

Molecular simulation is an important research method to study the structure and properties [55-59] of molecules or molecular systems through computer simulation which

based on Newtonian mechanism, including molecular mechanics (MM), Monte Carlo (MC) simulation, molecular dynamics (MD) simulation, etc. These methods are all based on the classical mechanical model of molecules or molecular systems, or obtain the stable configuration (MM) of molecules by optimizing the total energy of a single molecule; or by repeatedly sampling the configuration space of the molecular system and calculating its total energy, obtain the most probable configuration and thermodynamic equilibrium properties (MC) of the system; or obtain the phase trajectory of the system by numerically solving the classical mechanics equation of motion of the molecular system, and count the structural characteristics and properties (MD) of the system [60-62]. A simple schematic diagram of heating copper simulation snapshots is shown in Figure 1-2. At present, due to the development of molecular simulation theory, methods and computer technology, molecular simulation has become the third method to understand the world at the molecular level after experiments and theoretical methods [63-65].

The earliest MD simulations were implemented in 1957. Alder and Wainwright used computer simulations to study the motion of molecular systems ranging from 32 to 500 rigid spheres [66]. In 1964, Rahman [67] simulated and studied 864 Ar atomic systems with Lennard-Jones potential function, and obtained the properties related to the equation of state, radial distribution function, velocity autocorrelation function, mean square displacement, etc. Since then, with the efforts of molecular simulation researchers, the relationship between the Lennard-Jones potential function parameters and the model molecular architecture and properties has been established, which has had a profound

impact on molecular dynamics. Other researchers have also made great contributions to the development of molecular dynamics, such as in 1984, Kinetic methods at constant temperature; in 1991, molecular dynamics methods for the grand canonical ensemble. etc [68, 69].

To get the trajectory of the atom, besides the atomic mass, initial position, initial speed and other values that can be set artificially, the essential difference between different research objects lies in the force function (interaction/force field), the parameters of the force function determine the properties and behavior of the research objects, such as Lennard-Jones potential function mentioned above, used to describe the interaction of any two non-bonded atoms within the cut-off radius. The interaction between the bonding atoms is described by the bonding potential function. The bonding interaction is divided into bond energy, angle energy, dihedral energy, and improper energy, different molecules will have different bond potential energies. The more common bonding potential used to describe bonding atoms, such as CHARMM generalized, OPLS-AA, GAFF, these potential functions calculate the density and evaporation enthalpy of various organic molecules accurately, there are also force fields used to deal with reactions such as reaxff, REBO; the selection of a suitable potential function will affect on the results accuracy.

Currently there are many kinds of software for molecular simulation, Gromacs, NAMD, Amber and LAMMPS. LAMMPS (Large-scale Atomic/Molecular Massively Parallel Simulator) is a very popular simulation calculation software, the advantages of

LAMMPS are: single-core or multi-core high-performance computing; inserting new force fields and commands is very simple; can be coupled with other computing software; covering almost all particle models and force fields, etc. its shortcomings are also obvious: there is no visual interface; it cannot build more complex models and it cannot automatically assign force field parameters (Packmol and Moltemplate software are usually used for modeling and importing force field). LAMMPS has been used in many fields: chemistry, biomedicine, materials science and engineering, physics, etc [70-73].

The application prospect of molecular dynamics is very broad, and it plays an important role in predicting experimental conditions, predicting results, and analyzing results from a microscopic perspective.

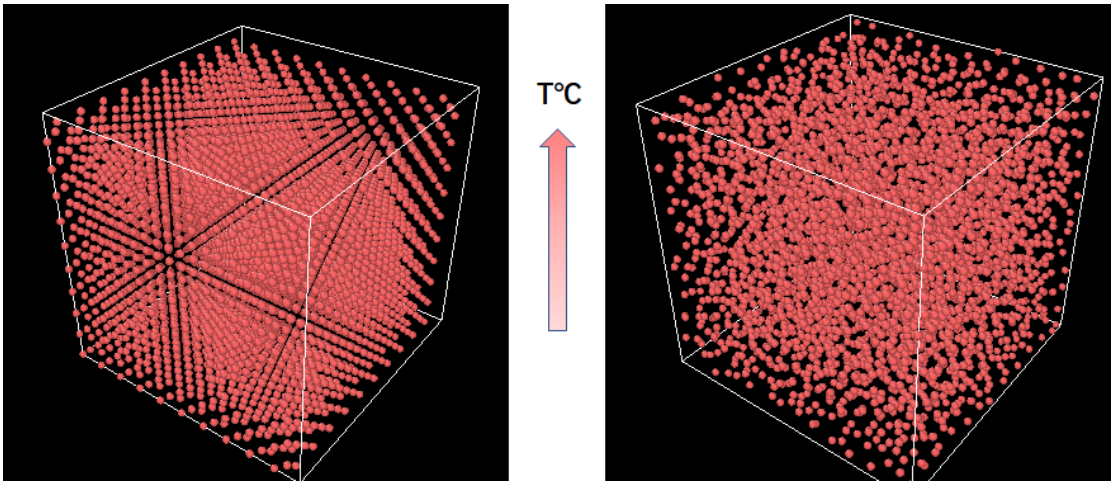

Figure 1-2 A schematic of copper melting simulation.

1.4 Polymers

A Polymer literally means many parts. It is a specific thing, usually a molecule or material made of smaller repeating units which are called monomer. [74], polymer is a

compound with a molecular mass of several thousand to several million, despite their high relative molecular mass, they are all connected in simple building blocks and repeats.

Polymers have a wide range of applications and can be seen everywhere in life (figure 1-3), such as by synthesizing valuable plastic products, etc. There are also naturally occurring polymers, such as proteins, which are natural polymers composed of amino acids, while nucleic acids (DNA and RNA) are nucleosides. Polymers of acids - such as complex molecules composed of nitrogenous bases, sugars, and phosphoric acids.

Polymers have been studied as early as the 19th century, in 1839, C. Goodyear discovered the vulcanization reaction of rubber, thus making a key progress in the research of making natural rubber a practical engineering material; in 1870 the industrialization of nitrocellulose plastics; in the 1950s, K. Ziegler and G. Natta discovered polymer coordination catalysts, ushering in the era of synthetic stereoregular structure polymers [75, 76]. With the improvement of people's understanding of polymers, synthetic polymers have achieved rapid development, and many important polymers have been industrialized.

Polymers have unique properties, depending on the type of molecules being bound and how they are bound. High elastic deformation [77] and viscoelasticity [78] are polymer-specific mechanical properties, some polymers are bendable and stretchable, such as rubber and polyester. Others are hard and tough, such as epoxy and glass; Heat resistance is an important indicator of the use temperature range of polymers [79, 80], and glass transition temperature and melting point are heat resistance indicators to

measure the physical deformation of amorphous and crystalline polymers, respectively; Dielectric constant, dielectric loss, breakdown voltage, etc [81-86]. can measure the electrical insulation of polymers. For example, non-polar polymers such as polyethylene and polytetrafluoroethylene are excellent high-frequency insulating materials [87], most polymers have good electrical insulating properties. In addition, the density of the polymer is small, which is much lighter than the steel of the same volume; some have good air tightness; some have electrical conductivity, semiconducting properties [88-91], low temperature resistance and radiation resistance, etc. These properties have been widely used in related industrial technology fields.

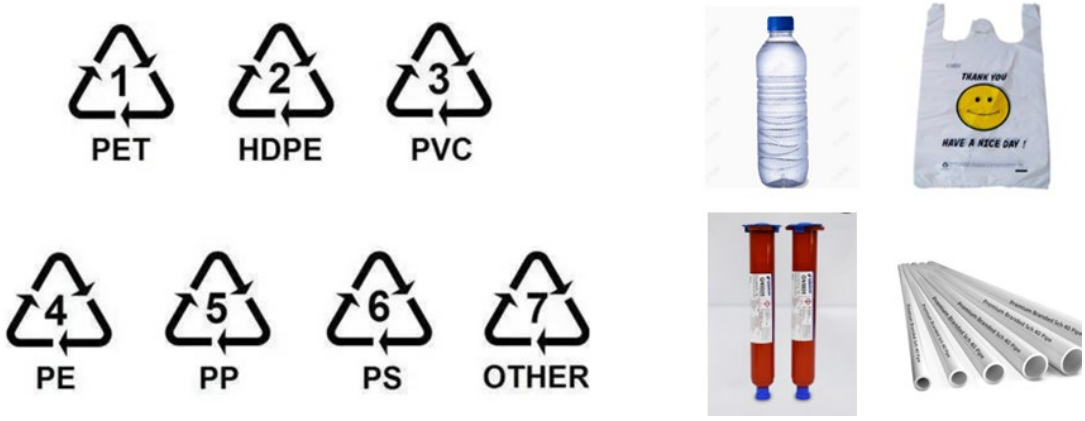

Figure 1-3 Polymer products in life.

1.5 Materials selection

First, I describe the materials used in Chapter 2, in Chapter 2 pentacene and naphthalene were used to fabricate pentacene crystals through naphthalene flux method. Pentacene ($C_{14}H_{22}$) is an important flexible electronic device material which belongs to

functional organic material. Due to pentacene stands out for its relatively high field effect mobility, the hole mobility of pentacene is as high as 35 cm^2 / (V·s) [92], which exceeds amorphous silicon. so that pentacene is mainly used in the preparation of organic thin film transistors. In the field of microelectronics, pentacene is a promising organic compound. Physical vapor transport (PVT) techniques are primarily used for single crystal growth of molecules including pentacene in device applications [93,94], Many research institutions have focused their research on the development of soluble pentacene precursors. After forming a film by dissolving, the precursor is decomposed into pentacene by heating, and finally a pentacene film with excellent performance is prepared. Since pentacene is insoluble in most organic solvents, it is slightly soluble in hot benzene solutions [95], therefore, finding a suitable solvent for pentacene is the key to the fabrication of pentacene crystals by liquid phase growth.

Naphthalene is an organic compound with formula $C_{10}H_8$, which is well known as the main ingredient of traditional mothballs [96]. Naphthalene can be as a precursor to other chemicals, such as phthalic anhydride, 1-naphthyl-N-methylcarbamate (carbaryl) [97]. The melting point of naphthalene is 80.2℃, molten naphthalene provides an excellent solubilizing medium for poorly soluble aromatic compounds, organic materials with conjugated π bond like 2′,2‴,3′,3‴,5′,5‴,6′,6‴-Octaphenyl-*p*-quinquepheny (OPQP), pentacene etc. have a good solubility in naphthalene [98, 99]. In many cases it is more efficient than other high-boiling solvents, such as dichlorobenzene, benzonitrile, nitrobenzene and durene.

Second, C_{60} is another important organic functional materials, in Chapter 3, C_{60} was selected as my research material, with the same treatment as pentacene, during the fabrication an anomalous phenomenon was found. C_{60} has metallic luster ad has many excellent properties, such as superconductivity strong magnetism, high pressure resistance, chemical resistance C_{60} film as a matrix material can be used to make a tooth-shaped combination capacitor. The chemical sensor made with it has the advantages of smaller size, simpler, renewable, and low price than traditional sensors [100] and may become an attractive on candidate products. In 1991, it was found that potassium doped C_{60} has superconducting behavior at 18K [101], which is the highest molecular superconducting temperature so far. After that, the superconducting properties of many metal-doped fullerenes were discovered. C_{60} and its derivatives not only have research value in superconductors, but also have potential application prospects in the fields of optical materials, magnetism, and biology materials etc [102-104].

Third, Poly (ether-ether-ketone) (PEEK) was used in Chapter 4, here molecular dynamic were combined with reported experiment results to understand the mechanisms of low wavenumber Raman spectroscopy and X-ray diffraction. PEEK [105-107] is a high-performance thermoplastic and crystalline polymer with excellent properties such as high temperature resistance and chemical resistance. It can be used as high temperature resistant structural material and electrical insulating material and can be compounded with glass fiber or carbon fiber to prepare reinforcing material. PEEK has numerous applications in aerospace, medical devices (as artificial bone to repair bone defects) and

in industry [108-111]. The processing conditions of PEEK can affect the crystallinity of the product and thus its properties. There are various methods to characterize the crystallinity of PEEK, such as Wide-angle X-ray diffraction, Raman microscopy etc [112-115]. but detailed understanding of the spectra has not been established. The discussed materials are shown in figure 1-4.

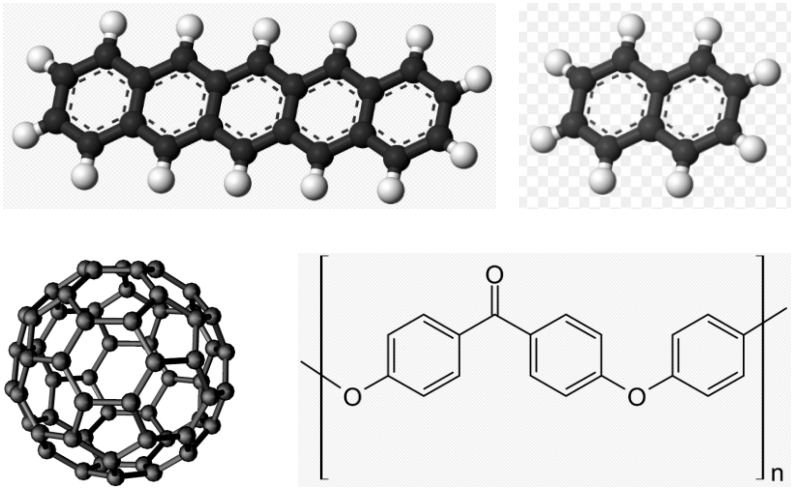

Figure 1-4 Pentacene, naphthalene, C_{60} and poly (ether ether ketone).

1.6 Objective of this dissertation

This dissertation is organized as follows:

Chapter 1 is the general introduction.

Chapter 2 is about the growth of pentacene crystals by "naphthalene flux method". Naphthalene flux method is a newly developed technique to grow crystals of molecules from a solution of naphthalene, and can be applied to large aromatic molecules that are insoluble to ordinary solvent. The pentacene is one of such molecules and a prototypical organic semiconductor. The solubility of pentacene in naphthalene was evaluated by

optical absorption at elevated temperature first, to determine the suitable solubility and temperature for pentacene crystal growth, then the obtained pentacene crystals were characterized by Laser microscopy, X-ray diffraction and poly figure to analysis the pentacene crystal structure.

Chapter 3 is about the anomalous effect of C_{60} and naphthalene, which was found in the attempt of grow C_{60} by the naphthalene flux method. C_{60} as an organic semiconductor material was trying to growth from naphthalene solution. I found the anomalous phenomenon of C_{60} in naphthalene unexpected. As the temperature increases, as the general experience, the solubility of organic compounds in organic solvents will increase, but C_{60} has an anomalous phenomenon. I improved the instrument for solubility measurement device to demonstrate this phenomenon by measuring the concentration of naphthalene vapors; At the same time, I used Packmol, moltemplate software to establish a mixture model, then simulate the mixture heating process with LAMMPS packages to observe this phenomenon from the microscopic point of view of simulation dynamics.

Chapter 4 is about the new technique to evaluate the vibrational spectra by molecular dynamics simulations and its comparison with the reported experiment about the composite of an engineering polymer PEEK with carbon fibers. Molecular dynamics simulation is used to demonstrate the existing experimental results. I use molecular dynamics combined with a newly developed approximation to simulate Raman spectroscopy to understand the effect of PEEK intermolecular ordering in the spectra. I found that PEEK intermolecular ordering does affect the low wavenumber Raman spectra

and the x-ray diffraction as observed in the experiment. Combining the results of experiments and simulations can illustrate experimental results or phenomena from multiple perspectives.

Chapter 5 gives the general conclusion of research topics covered by dissertation.

Reference

1. Chung D D L. Springer Science & Business Media, 2003.
2. Eliseeva S V, Bünzli J C G. Chemical Society Reviews, 2010, 39(1): 189-227.
3. Cui, Y., Li, B., He, H., Zhou, W., Chen, B., Qian, G. Accounts of chemical research, 2016, 49(3): 483-493.
4. Cheng, F., Liang, J., Tao, Z., Chen, J. Advanced materials, 2011, 23(15): 1695-1715.
5. Mattevi, C., Eda, G., Agnoli, S., Miller, S., Mkhoyan, K. A., Celik, O., Mastrogiovanni, D., Granozzi, G. Grafunkel, E., Chhowalla, M. Advanced Functional Materials, 2009, 19(16): 2577-2583.
6. Khazaei, M., Arai,M., Sasaki, T., Chung, C. Y., Venkataramanan, N. S., Estili, M., Sakka,Y., Kawazoe, Y. Advanced Functional Materials, 2013, 23(17): 2185-2192.
7. Pileni M P. Advanced Functional Materials, 2001, 11(5): 323-336.
8. Kai, D., Tan, M. J., Chee, P. L., Chua, Y. K., Yap, Y. L., Loh, X. J. Green Chemistry, 2016, 18(5): 1175-1200.
9. Ikkala O, ten Brinke G. science, 2002, 295(5564): 2407-2409.
10. Hlasnik, I., Takacs, S., Burjak, V. P., Majoroš, M., Krajčik, J., Krempaský, Ľ., M.Polák., M.Jergel., T. A. Korneeva., O. N. Mironova., Ivan, I. Cryogenics, 1985, 25(10): 558-565.
11. Jouve G, Séverac C, Cantacuzene S. Thin Solid Films, 1996, 287(1-2): 146-153.
12. Scanlan R M, Fietz W A, Koch E F. Journal of Applied Physics, 1975, 46(5): 2244-

2249.

13. Clarke. J, Braginski. A. I. Weinheim: Wiley-Vch, 2004.
14. Pickett. W. E. Reviews of Modern Physics, 1989, 61(2): 433.
15. R. L. Sandstrom, W. J. Gallagher, T. R. Dinger, R. H. Koch, R. B. Laibowitz, A. W. Kleinsasser, R. J. Gambino, B. Bumble, and M. F. Chisholm. Applied physics letters, 1988, 53(5): 444-446.
16. Schwartz, J., Effio, T., Liu, X., Le, Q. V., Mbaruku, A. L., Schneider-Muntau, H. J., Weijers, H. W. IEEE Transactions on Applied Superconductivity, 2008, 18(2): 70-81.
17. R. R. King, D. C. Law, K. M. Edmondson, C. M. Fetzer, G. S. Kinsey, H. Yoon, R. A. Sherif, and N. H. Karam. Applied physics letters, 2007, 90(18): 183516.
18. R. R. King,D. Bhusari,D. Larrabee,X.-Q. Liu,E. Rehder,K. Edmondson,H. Cotal,R. K. Jones,J. H. Ermer,C. M. Fetzer,D. C. Law,N. H. Karam. Progress in Photovoltaics: Research and Applications, 2012, 20(6): 801-815.
19. Cornwell D J, Smith D K. Materials Horizons, 2015, 2(3): 279-293.
20. Newnham R E, Ruschau G R. Journal of the American Ceramic Society, 1991, 74(3): 463-480.
21. Gandhi M V, Thompson B D. Springer Science & Business Media, 1992.
22. Ashima, R., Haleem, A., Bahl, S., Javaid, M., Mahla, S. K., & Singh, S. Materials Today: Proceedings, 2021, 45: 5081-5088.
23. C.L. Thomas; T.M. Gaffney; S. Kaza; C.H. Lee. 1996 IEEE Aerospace Applications

Conference. Proceedings. IEEE, 1996, 4: 219-230.

24. Chiang, C. K., Fincher Jr, C. R., Park, Y. W., Heeger, A. J., Shirakawa, H., Louis, E. J., Gau, C. S., MacDiarmid, A. G. Applied Surface Science, 2000, 166(1-4): 354-362.

25. Hill, I. G., Milliron, D., Schwartz, J., Kahn, A. Applied Surface Science, 166(1-4), 354-362.

26. Virkar, A. A., Mannsfeld, S., Bao, Z., Stingelin, Advanced Materials, 2010, 22(34): 3857-3875.

27. Rivnay, J., Mannsfeld, S. C., Miller, C. E., Salleo, A., Toney, M. F. Chemical reviews, 2012, 112(10): 5488-5519.

28. H. E. Katz, A. J. Lovinger, J. Johnson, C. Kloc, T. Siegrist, W. Li, Y.-Y. Lin A. Dodabalapur, Nature, 2000, 404(6777): 478-481.

29. Fei, H., Dong, J., Arellano-Jiménez, M. J., Ye, G., Dong Kim, N., Samuel, E. L., Tour, J. M. Nature communications, 2015, 6(1): 1-8.

30. Ghosh, I., Khamrai, J., Savateev, A., Shlapakov, N., Antonietti, M., König, B. Science, 2019, 365(6451): 360-366.

31. Gao Y. Materials Science and Engineering: R: Reports, 2010, 68(3): 39-87.

32. Dediu, V., Murgia, M., Matacotta, F. C., Taliani, C., & Barbanera, S. Solid State Communications, 2002, 122(3-4): 181-184.

33. Wu, Y., Yan, H., Huang, M., Messer, B., Song, J. H., Yang, P. Chemistry–A European Journal, 2002, 8(6): 1260-1268.

34. S. Niki, M. Contreras, I. Repins, M. Powalla, K. Kushiya, S. Ishizuka and K. Matsubara, Prog. Photovoltaics, 18, 453 (2010).

35. P. Jackson, D. Hariskos, E. Lotter, S. Paetel, R. Wuerz, R. Menner, W. Wischmann and M. Powalla, Progress in Photovoltaics: Research and Applications, 19, 894 (2011).

36. Sun, Y., Khang, D. Y., Hua, F., Hurley, K., Nuzzo, R. G., Rogers, J. A. Advanced Functional Materials, 2005, 15(1): 30-40.

37. Snyder G H, Matichenkov V V, Datnoff L E. CRC Press, 2016: 567-584.

38. Melville O A, Grant T M, Lessard B H. Journal of Materials Chemistry C, 2018, 6(20): 5482-5488.

39. Dominey, R. N., Lewis, N. S., Bruce, J. A., Bookbinder, D. C., & Wrighton, M. S. Journal of the American Chemical Society, 1982, 104(2): 467-482.

40. Castilho, J. H., Chambouleyron, I., Marques, F. C., Rettori, C., & Alvarez, F. Physical Review B, 1991, 43(11): 8946.

41. Noguchi, Y., Sekitani, T., Yokota, T., Someya, T. Applied Physics Letters, 2008, 93(4): 273.

42. Bronstein, H., Nielsen, C. B., Schroeder, B. C., McCulloch, I. Nature Reviews Chemistry, 2020, 4(2): 66-77.

43. Nelson, S. F., Lin, Y. Y., Gundlach, D. J., Jackson, T. N. Applied physics letters, 1998, 72(15): 1854-1856.

44. Klauk, H., Halik, M., Zschieschang, U., Schmid, G., Radlik, W., Weber, W. Journal

of Applied Physics, 2002, 92(9): 5259-5263.

45. Giri, G., Park, S., Vosgueritchian, M., Shulaker, M. M., Bao, Z. Advanced materials, 2014, 26(3): 487-493.

46. Park, S. K., Jackson, T. N., Anthony, J. E., & Mourey, D. A. Applied Physics Letters, 2007, 91(6): 063514.

47. Kato, Y., Iba, S., Teramoto, R., Sekitani, T., Someya, T., Kawaguchi, H., Sakurai, T. Applied physics letters, 2004, 84(19): 3789-3791.

48. Wei, W., Yang, C., Mai, J., Gong, Y., Yan, L., Zhao, K., Liu, J. M. (2017). Journal of Materials Chemistry C, 2017, 5(40): 10652-10659.

49. Nathan, A., Ahnood, A., Cole, M. T., Lee, S., Suzuki, Y., Hiralal, P., Milne, W. I. IEEE. 100, 1486-1517 (2012)

50. Hu, B., Li, D., Manandharm, P., Fan, Q., Kasilingam, D., Calvert, P. Journal of Materials Chemistry, 2012, 22(4): 1598-1605.

51. Chen C Q, Zhu J. Applied physics letters, 2007, 90(4): 043105.

52. Podzorov V, Pudalov V M, Gershenson M E. Applied physics letters, 2003, 82(11): 1739-1741.

53. Takeya, J., Goldmann, C., Haas, S., Pernstich, K. P., Ketterer, B., Batlogg, B. Journal of applied physics, 2003, 94(9): 5800-5804.

54. Yuan, Y., Giri, G., Ayzner, A. L., Zoombelt, A. P., Mannsfeld, S. C., Chen, J., Bao, Z. Nature Communications, 2014, 5(1):3005.

55. Gilbert N. Sociological research online, 1997, 2(2): 91-105.

56. Head-Gordon T, Hura G. Chemical reviews, 2002, 102(8): 2651-2670.

57. Soper A K. Chemical Physics, 1996, 202(2-3): 295-306.

58. Ermak D L. The Journal of Chemical Physics, 1975, 62(10): 4189-4196.

59. Cheung P S Y, Powles J G. Molecular Physics, 1975, 30(3): 921-949.

60. Zgarbová, M., Otyepka, M., Šponer, J., Hobza, P., Jurečka, P. Physical Chemistry Chemical Physics, 2010, 12(35): 10476-10493.

61. Kroese, D. P., Brereton, T., Taimre, T., Botev, Z. I. Computational Statistics, 2014, 6(6): 386-392.

62. Schlick T. NY, 1996: 219-247.

63. Payne, M. C., Teter, M. P., Allan, D. C., Arias, T. A., Joannopoulos, A. J. Reviews of modern physics, 1992, 64(4): 1045.

64. Van Gunsteren W F, Berendsen H J C. Angewandte Chemie International Edition in English, 1990, 29(9): 992-1023.

65. Cygan R T. Molecular Modeling Theory: Applications in the Geosciences, 2001, 42: 1-35.

66. Alder B J, Wainwright T E. The Journal of chemical physics, 1957, 27(5): 1208-1209.

67. Rahman A. Physical review, 1964, 136(2A): A405.

68. Weitz, D. A., Huang, J. S., Lin, M. Y., Sung, J. Physical Review Letters, 1984, 53(17): 1657.

69. Altshuler B L, Gefen Y, Imry Y. Physical review letters, 1991, 66(1): 88.

70. Viani, L., Risko, C., Toney, M. F., Breiby, D. W., Bredas, J. L. ACS nano, 2014, 8(1): 690-700.

71. Jolfaei, N. A., Jolfaei, N. A., Hekmatifar, M., Piranfar, A., Toghraie, D., Sabetvand, R., Rostami, S. Computer methods and programs in biomedicine, 2020, 185: 105169.

72. Cantrell R, Clancy P. Surface science, 2008, 602(22): 3499-3505.

73. Wong-Ekkabut, J., Baoukina, S., Triampo, W., Tang, I. M., Tieleman, D. P., Monticelli, L. Nature nanotechnology, 2008, 3(6): 363-368.

74. Morawetz H. Rubber chemistry and technology, 2000, 73(3): 405-426.

75. Feldman D. Designed monomers and polymers, 2008, 11(1): 1-15.

76. Dufaud V, Basset J M. Angewandte Chemie International Edition, 1998, 37(6): 806-810.

77. Monroe C, Newman J. Journal of The Electrochemical Society, 2005, 152(2): A396.

78. Brinson H F, Brinson L C. An introduction, 2008: 99-157.

79. Hashima K, Nishitsuji S, Inoue T.Polymer, 2010, 51(17): 3934-3939.

80. Giannelis E P. Applied organometallic chemistry, 1998, 12(10-11): 675-680.

81. Maier G. Progress in polymer science, 2001, 26(1): 3-65.

82. Martin, S. J., Godschalx, J. P., Mills, M. E., Shaffer, E. O., Townsend, P. H. Advanced Materials, 2000, 12(23): 1769-1778.

83. Zhu L. The journal of physical chemistry letters, 2014, 5(21): 3677-3687.

84. Zimm B H. The journal of chemical physics, 1956, 24(2): 269-278.

85. Rao Y, Wong C P. Journal of Applied Polymer Science, 2004, 92(4): 2228-2231.

86. Pleşa, I., Noţingher, P. V., Schlögl, S., Sumereder, C., & Muhr, M. Polymers, 2016, 8(5): 173.

87. Hanley, T. L., Burford, R. P., Fleming, R. J., Barber, K. W. IEEE Electrical Insulation Magazine, 2003, 19(1): 13-24.

88. Miyasaka, K., Watanabe, K., Jojima, E., Aida, H., Sumita, M., Ishikawa, K. Journal of Materials Science, 1982, 17(6): 1610-1616.

89. Clingerman, M. L., King, J. A., Schulz, K. H., & Meyers, J. D. Journal of Applied Polymer Science, 2002, 83(6): 1341-1356.

90. Guo X, Facchetti A, Marks T J. Chemical reviews, 2014, 114(18): 8943-9021.

91. Xu, J., Wu, H. C., Zhu, C., Ehrlich, A., Shaw, L., Nikolka, M., Bao, Z. Nature materials, 2019, 18(6): 594-601.

92. Jurchescu, O. D., Popinciuc, M., Van Wees, B. J., & Palstra, T. T. Advanced Materials, 2007, 19(5): 688-692.

93. Laudise, R. A., Kloc, C., Simpkins, P. G., Siegrist, T. Journal of crystal growth, 1998, 187(3-4): 449-454.

94. T. Abe, R. Matsubara, M. Hayakawa, A. Shimoyama, T. Tanaka, A. Tsuji, Y. Takahashi, A. Kubono, Jpn. J. Appl. Phys. 2018, 57, 03EG13.

95. Fujikake, H., Suzuki, T., Isaka, F., Sato, F. Japanese journal of applied physics, 2004, 43(4B): L536.

96. Sudakin D L, Stone D L, Power L. Current topics in toxicology, 2011, 7: 13.

97. Headley J V, McMartin D W. Journal of Environmental Science and Health, Part A,

2004, 39(8): 1989-2010.

98. Yanase, T., Tanoguchi, H., Sakai, N., Jin, M., Yamane, I., Kato, M., Ito, H., Nagahama, T., Shimada, *Crystal Growth & Design*, **2021**, 21, 8, 4683-4689

99. Sakai, N., Tamura, T., Yanase, T., Nagahama, T., Shimada, *Japanese Journal of Applied Physics,* **2019**, 58, SBBG08

100. Liu, Z., Wang, H., Li, J., Wang, M., Yang, H., Si, F., Kong, J. Microchemical Journal, 2021, 170: 106772.

101. Hebard, A., Rosseinky, M., Haddon, R., Murphy, D., Glarum, S., Palstra, T., Karton, A. Nature, 1991, 350: 600-601.

102. Lyon, D. Y.; Brown, D. A.; Alvarez, P. J. J. Water Sci. Technol., 2008, 57, 1533–1538

103. Tanigaki, K., Ebbesen, T. W., Saito, S., Mizuki, J., Tsai, J. S., Kubo, Y., Kuroshima, S. Nature, 1991, 352(6332): 222-223.

104. Tutt L W, Kost A. Nature, 1992, 356(6366): 225-226.

105. Jones D P, Leach D C, Moore D R. Polymer, 1985, 26(9): 1385-1393.

106. Cebe P, Hong S D. Polymer, 1986, 27(8): 1183-1192.

107. Xing, P., Robertson, G. P., Guiver, M. D., Mikhailenko, S. D., Wang, K., Kaliaguine, S. Journal of membrane science, 2004, 229(1-2): 95-106.

108. Li H, Englund K. Journal of composite materials, 2017, 51(9): 1265-1273.

109. Amanat, N., Chaminade, C., Grace, J., McKenzie, D. R., James, N. L. Materials & design, 2010, 31(10): 4823-4830.

110. Toth, J. M., Wang, M., Estes, B. T., Scifert, J. L., Seim III, H. B., Turner, A. S. Biomaterials, 2006, 27(3): 324-334.

111. Panayotov, I. V., Orti, V., Cuisinier, F., Yachouh, J. Journal of Materials Science: Materials in Medicine, 2016, 27(7): 1-11.

112. Doumeng, M., Makhlouf, L., Berthet, F., Marsan, O., Delbé, K., Denape, J., Chabert, F. Polymer Testing, 2021, 93: 106878.

113. Xue S, Yin G. Polymer, 2006, 47(14): 5044-5049.

114. Puértolas, J. A., Castro, M., Morris, J. A., Ríos, R., Ansón-Casaos, A. Spectrochimica Acta Part A: Molecular Spectroscopy, 1991, 47(9-10): 1299-1303.

115. Stuart B H. Spectrochimica Acta Part A: Molecular and Biomolecular Spectroscopy, 1997, 53(1): 107-110.

Chapter 2

Growth of pentacene crystals by naphthalene flux method

2.1 Introduction

Organic semiconductors have several advantages like flexible, low-cost and printable electronic circuits [1-9], It is necessary to design and synthesize molecules with a high performance for such applications, but there are still some "missing links" connecting molecular structures and the physical properties of the organic semiconductor materials, such as exciton binding energies, lifetime, carrier mobilities, etc. It is necessary to find a way to relate molecular structure to important physical properties as semiconductors and various applications summarized in recent reviews [9,10] by fabricating organic semiconductor crystals and experimentally studying their crystal structures and various physical properties.

Pentacene ($C_{14}H_{22}$) is an important organic semiconductor from the early days of research [11-25]. Pentacene stands out for its relatively high field effect mobility. Its hole mobility is as high as 35 $cm^2/(V \cdot s)$ in one report [19], which exceeds amorphous silicon.

In this research, I aimed to grow pentacene crystals by a new method called "naphthalene flux method" [26]. The method uses a solid aromatic molecule (naphthalene; melting point 80.2 ℃) as a solvent or flux for pentacene. It is well known that pentacene decomposes above its melting point, so melt growth techniques cannot be applied. Physical vapor transport (PVT) techniques are primarily used for single crystal growth of molecules including pentacene in device applications [27-29]. Pentacene has poor solubility in common organic solvents [30]. Transistors were fabricated by growing

pentacene thin film crystals from 1,2,4-trichlorobenzene solution at 140 ℃ [31-33], but the size of the crystals was quite inferior than that obtained by PVT.

I searched for the solvent of pentacene through experiments and found that pentacene could be dissolved in naphthalene solution. The growth of crystals in solution will be easier to control, and the crystal size obtained by the "naphthalene flux method" is comparable or larger than that is obtained by the PVT method.

2.2 Experimental section

2.2.1 Solubility measurement

The temperature that is suitable for pentacene crystal growth were determined first by measuring the solubility of pentacene in naphthalene. I measured the optical absorption of heated solutions of pentacene in naphthalene with excess amounts of pentacene. Since the optical density of a pentacene solution is high, the thickness of the solution must be thin. I used a glass capillary (2.4 mm inner diameter) to hold the solution. This requires handling of a very tiny amount of pentacene. Therefore, the typical procedure was as follows:

A glass tube was prepared which contained about 1 mg of pentacene and 100 μl of chlorobenzene, then pumped to 10 Pa and sealed by melting the glass tube, then the glass tube was heated to 120℃ to dissolve the pentacene, a clear purple solution can be observed, then the glass tube was opened and 20 μl of the solution was transferred to the capillary by a micropipette while it was hot, and the chlorobenzene was evaporated with

pumping at about 140℃, finally, about 0.4 g naphthalene was added to the capillary and the capillary was vacuum sealed.

The prepared capillary sample was placed in a temperature-controlled aluminum block, which had a light able to pass through both sides (Fig. 2-1). when heating the aluminum block the temperature will gradually raise up, at about 80℃, the naphthalene will first melt, then pentacene will start to dissolve into the naphthalene, The optical absorption of the solution was measured by a white LED light source and microspectrometer (Hamamatsu C12880MA; with Color Compass software). I recorded the absorption spectra every 10 ºC. The concentration was calculated based on the Lambert-Beer formula:

$$log_{10}\,(I_0/I) = \varepsilon bc \qquad (1)$$

Where I_0 and I are the intensity (or power) of the incident light and the transmitted light, respectively. ε is the molar absorption coefficient, b is the light path (inner diameter of the capillary), and c is the concentration. I0 was measured by setting a capillary containing only naphthalene as a blank.

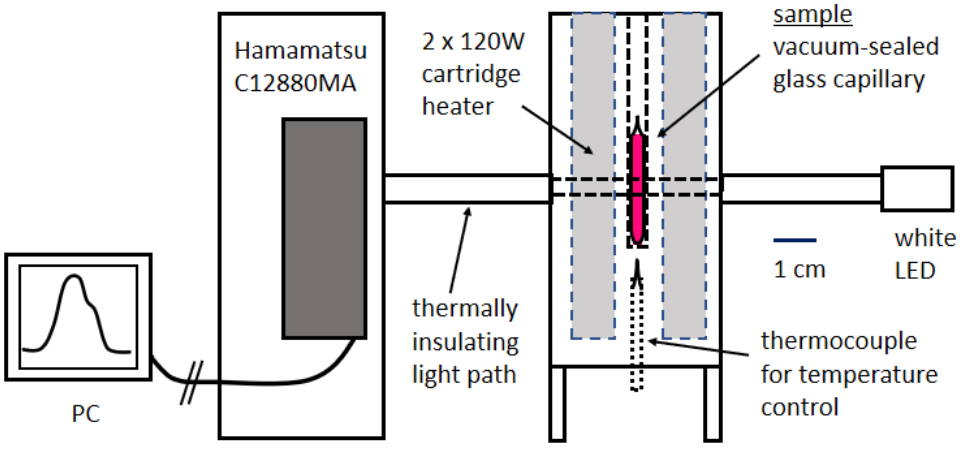

Figure 2-1 schematic of solubility measurement device.

2.2.2 Crystal growth

Naphthalene and pentacene are air sensitive at high temperature [34,35] and naphthalene is highly volatile [36,37], the growth process was performed in a vacuum sealed H-shape glass tube, in this experiment, the heater used for the H-shape glass tube can be separately controlled on both sides, The method is schematically illustrated in Fig. 2-2(a). (i) when raised temperature up on both sides, pentacene is dissolved into naphthalene. (ii) the temperature of right side was set a little lower than left side, and both sides were very slowly cooled. The pentacene crystal grew in the left side. The right side was cooled first before the naphthalene on the left side had solidified in order to collect the naphthalene on the right side by vapor transport. (iii) The left side contained the pentacene crystal and the naphthalene was completely collected on the right side. A typical temperature profile is shown in Fig. 2-2 (b). Some images about this experiment are shown in Fig. 2-2 (c).

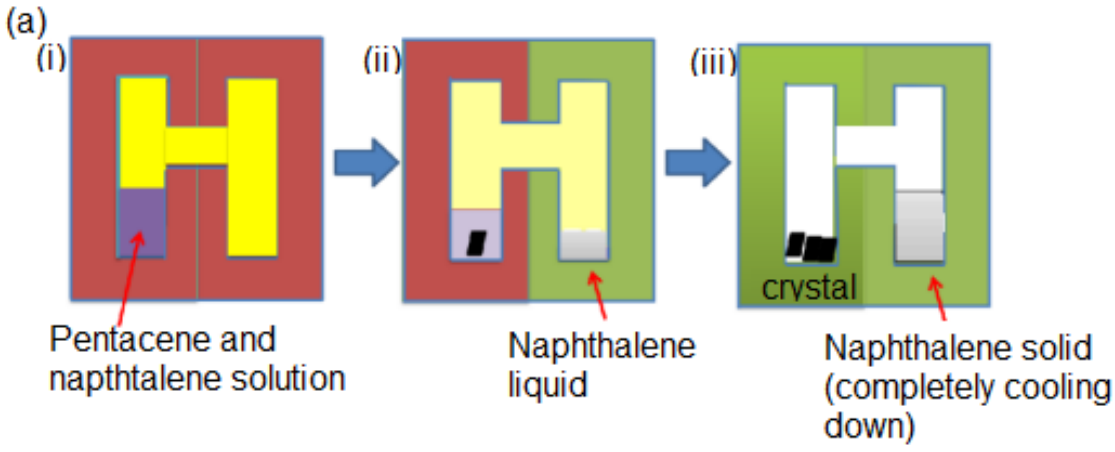

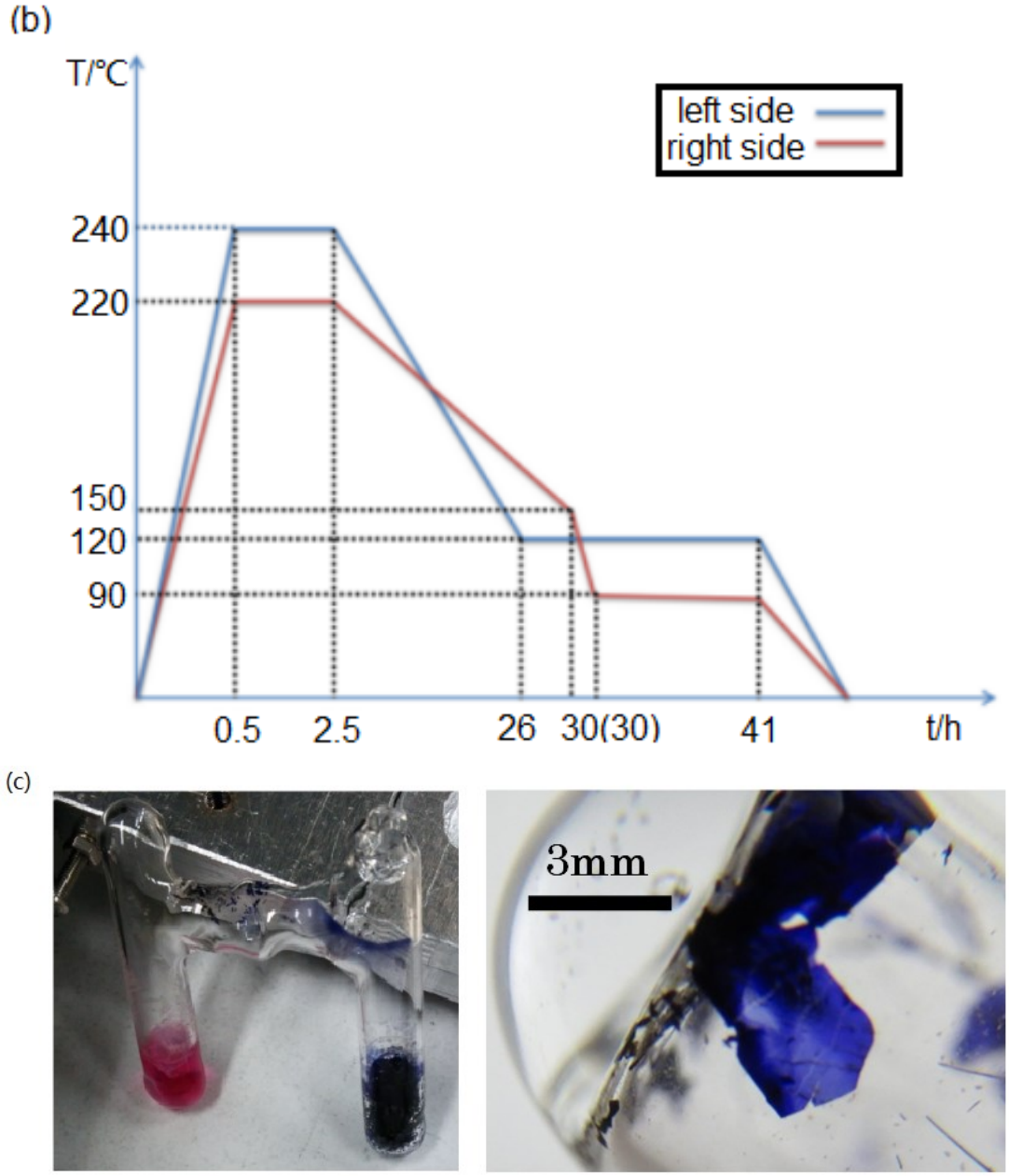

Figure 2-2: Crystal growth scheme. (a) Schematics of naphthalene flux method. (b) Temperature (*T*) -time(*t*) profiles of left and right sides. (c) Left: H-shaped glass tube taken out from the aluminum block heater while hot. Right: Pentacene crystal in the H-sheped tube (upper left is the bottom).

2.2.3 Characterization

The surface morphology of the pentacene crystal was observed by a laser microscope (Keyence KN-7200). Polarization optical microscopy (Olympus BX51) was used to evaluate the crystal orientation of the pentacene crystal. The θ-2θ (Rigaku Miniflex 600) and pole figure (Rigaku SmartLab) X-ray diffraction (XRD) were used to evaluate the crystallinity and the crystal structure.

2.3 Results and discussions

2.3.1 Solubility results

At room temperature the solubility of pentacene in naphthalene is low, the solubility of pentacene in naphthalene will gradually increase as the temperature increases, Figure 2-3(a) shows the sample used for the solubility measurement and Figure 2-3 (b) shows the obtained absorbance curve.

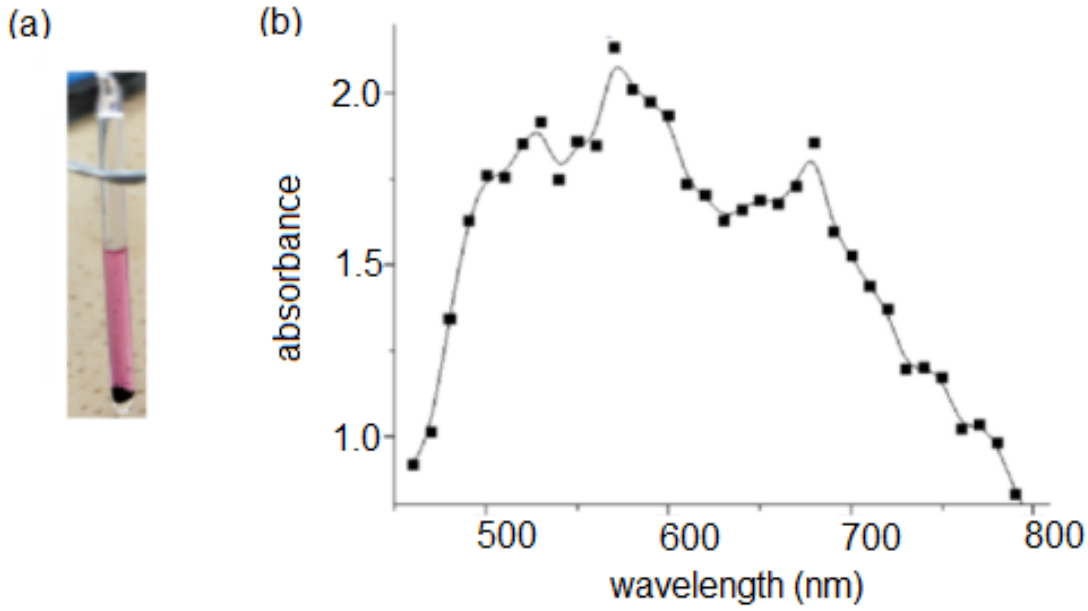

Figure 2-3. (a) Solubility measurement sample (pentacene-naphthalene at 90 ℃). (b) Absorbance spectrum of pentacene dissolved in naphthalene.

Figure 2-4 shows the optical absorbance at 528 nm of two samples which contained 0.20 and 0.15 wt% of pentacene in naphthalene as a function of temperature. The two curves were almost agreed at the lower temperatures, the curve of the sample which contained 0.15wt% pentacene became constant at about 230℃, it can be explained as follow:

At the beginning the concentration of pentacene in solution is approximately same, because all of the soluble pentacene is dissolved in an equilibrium with the pentacene solid. Then the solubility increases as the temperature increases, after pentacene completely dissolved into naphthalene, the curve became a straight line. The absorbance value of the straight line corresponds to εbc in Eq.(1). The concentration c can be calculated from the pentacene : naphthalene ratio charged in the capillary, b is the inner

diameter of the capillary, if assumed the molar absorption coefficient of pentacene in naphthalene is a constant, the ε can be evaluated from the shown data in Figure 2-4, which was ~ 1.1 x 10^3 L mol^{-1} cm^{-1}. Error remains in the ε value because it is difficult to estimate the light path in a capillary with accuracy.

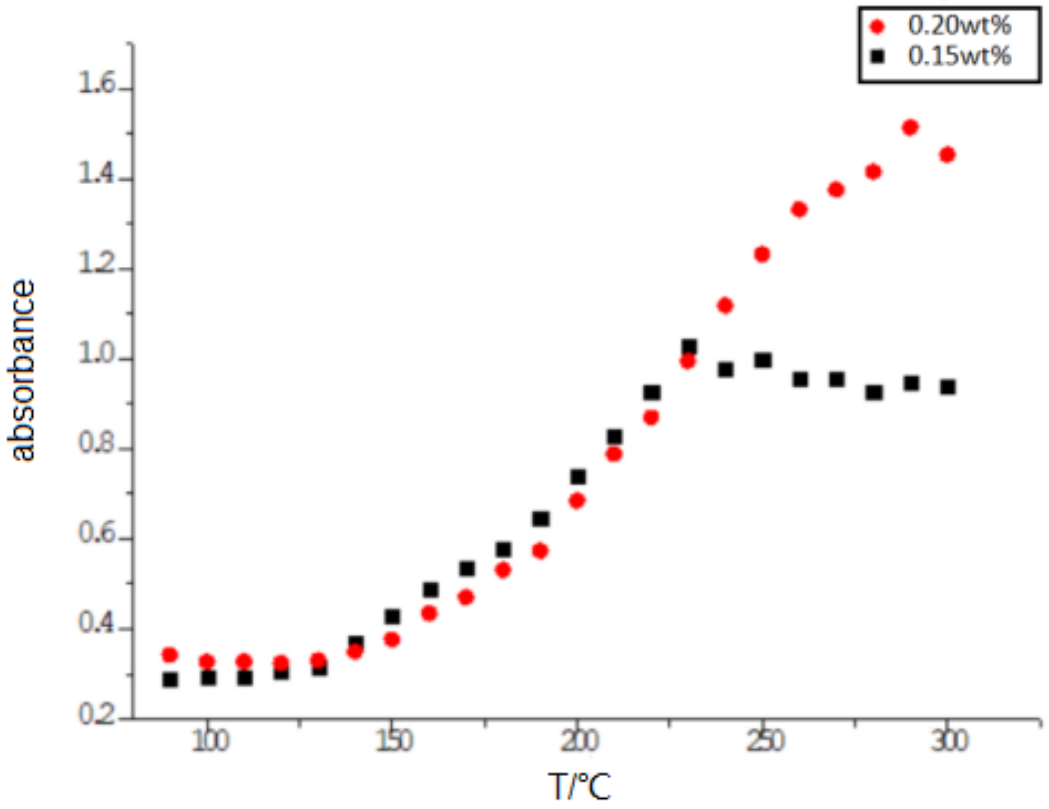

Figure 2-4. Solubility measurement curves of pentacene in naphthalene. (a) and (b) contain 0.20 wt% and 0.15 wt% pentacene in naphthalene, respectively.

2.3.2 Naphthalene flux method results

The obtained solubility and temperature data were used as the basis to determine the condition for crystal growth. A 0.15 wt% pentacene mixture with naphthalene was used, the temperature profile shown in Fig. 2-4 (b). The periods and temperatures in the profile

were determined on a trial-and-error-basis. At different maximum temperatures the obtained pentacene crystals are shown in Figure 2-5 (a), I found that pentacene crystals can be obtained at the highest temperatures of 220 ~ 240 ℃, and the largest crystal (about 1.1 cm) was obtained at 240 ℃. When the highest temperature is above 260 ℃, the results were not stable and most of the crystals were a powder. I picked the crystal with well-defined faces and removed any visible impurities under the microscope, then cleaned the surface with acetone for subsequent measurements. Figure 2-5 (b) shows a laser microscope image of a pentacene crystal in order to measure the thickness and evaluate the flatness of the surface. The thickness of crystal was about 14 μm, it is a plate-like crystal. A piece of the pentacene crystal was characterized by a polarization microscope Fig. 2-5 (c). We can see the change in the contrast by rotating the sample, which is caused by the optical anisotropy of the pentacene crystal.

2.3.3 Characterization

The sample was characterized by X-ray diffraction to determine the crystal structure. Figure 2-6 shows the out-of-plane (θ-2θ) scan x-ray diffraction. It shows periodic peaks corresponding to the layered stacking of the herringbone lattice of pentacene. There are more than 10 reported structures of pentacene, which are basically classified into three groups [38-43], *i.e.* the "bulk type" (layer spacing d =14.5Å; high temperature form), single crystal type (d =14.5Å; obtained by PVT), and "thin film type" (d =15.5Å; obtained by thin film deposition) . The differences in these structures are rather slight, but the

electronic band structure is very dependent on it [44]. We can rule out the possibility of "thin film phase" because the (0 0 1) diffraction appears below $2\theta = 6.0°$. From the out-of-plane scan, it is suggested that the "bulk type" is formed. But the large single crystals can be somewhat warped during the handling, the accuracy of interlayer spacing (d) from this XRD is not conclusive. The three-dimensional lattice parameters must be evaluated to confirm the crystal structure.

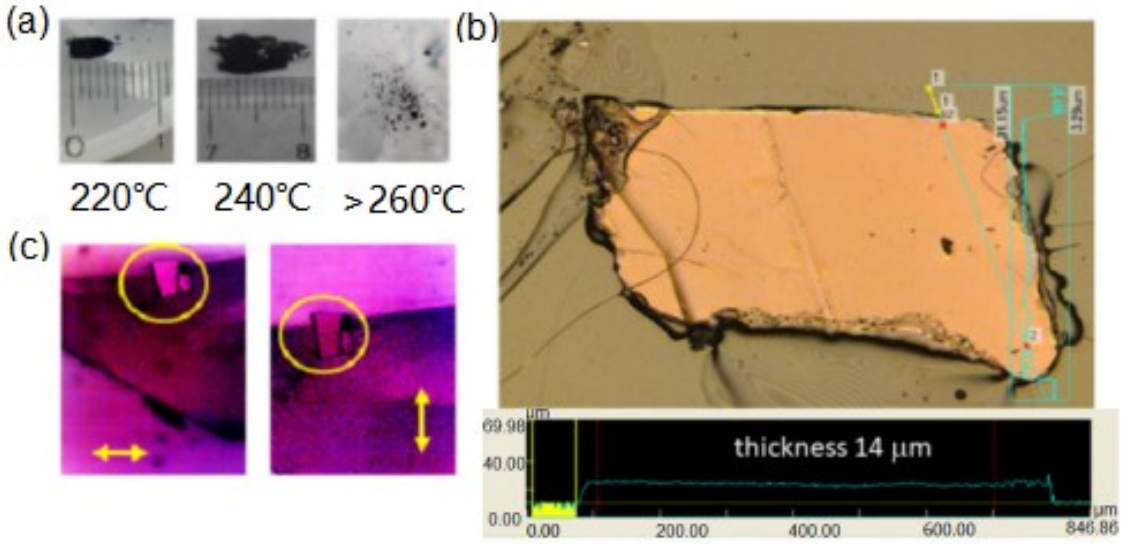

Figure 2-5. (a) Obtained pentacene crystals at different growth temperatures by flux evaporation method. (b) Laser microscope image of pentacene crystal. (c) Polarization microscope images of a pentacene crystal. The brightness of the crystal changed (see circle) when the dial was rotated 90°.

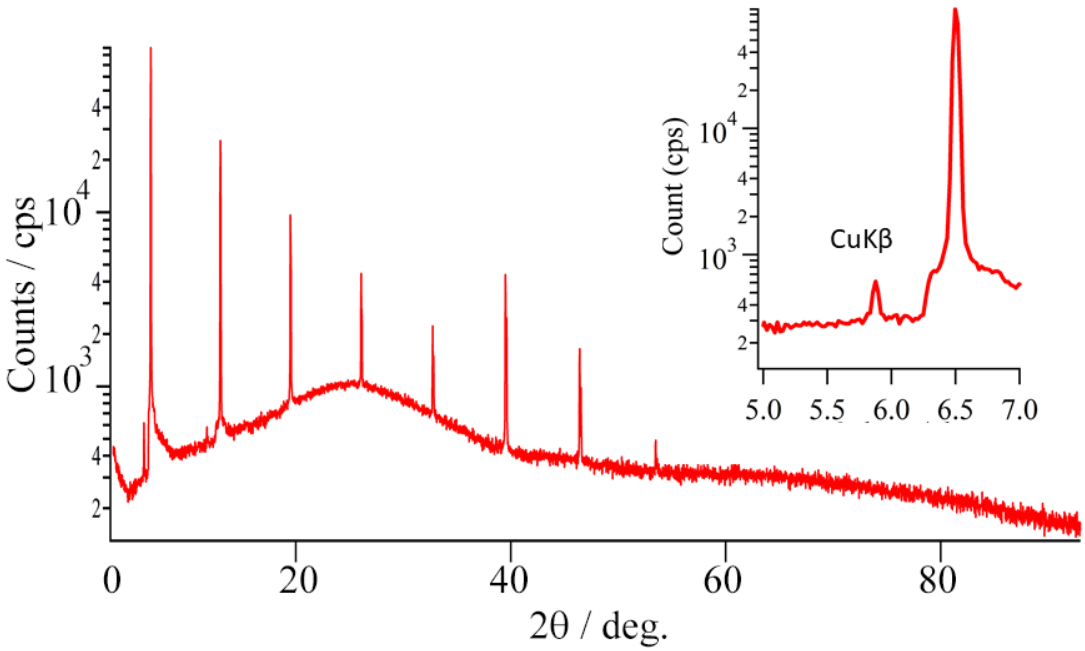

Figure 2-6. Out-of-plane X-ray diffraction of a pentacene plate-like crystal.

I measured a pole figure of the pentacene plate crystal by 5-axis XRD equipment (Fig. 2-7). 2θ was set to 17.7°, which corresponds to the (1 1 1) diffraction for the single crystal type and (1 0 -3) diffraction for the bulk type. The result is shown in Fig. 2-8. Four spots appeared. It shows that the plate-like pentacene crystal is made of twins. To analyze the orientations of the twins, I calculated the diffraction peaks of each polytype of pentacene near $2\theta = 17.7°$.

By calculating the reciprocal lattice of each unit lattice, I have identified the spots in the pole figure, which appeared 11 - 18° off from the surface normal (α), that is the (1 0 -3) diffraction of the "bulk type" pentacene ($\alpha = 16°$). The (1 1 1) diffraction of the "single crystal type" should appear at $\alpha = 69°$, which is distinctly different from the result.

As for the twin orientation, each {1 0 -3} diffraction is separated into two spots. This

means that the a* and/or c* axes are separated in the reciprocal space. Because the a-b plane of the layered structure should be common to explain the flatness of the crystal surface, the c* axis is also common. It follows that the b axis in the real space has different directions in the twin. Assuming that the a- axis is common, the ϕ (β) scan shown in Fig. 2-8, which shows a 12° separation of the two-fold symmetric peaks, can be reasonably explained. The model structure of the twins in the real space is Fig. 2-9. As mentioned in [46], the twin structure formed is attributed to the change in anisotropy of van der Waals interaction with simultaneous epitaxy. As for the size of each twin crystal, we could not resolve the distribution by geometrically scanning the XRD spot, which means it was smaller than the x-ray spot (0.5 mm) of the measurement. The detail of the XRD data analysis can be found in Table 1-4 and Figure 2-10.

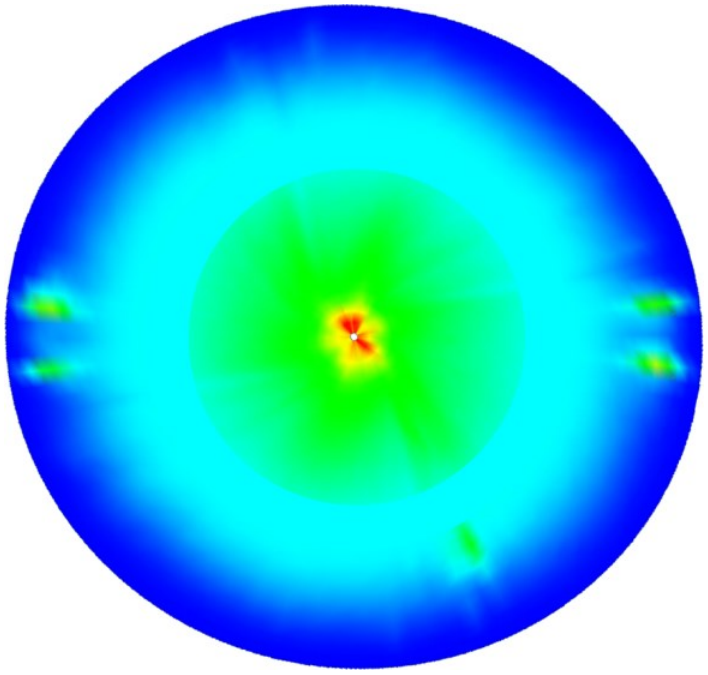

Figure 2-7. Pole figure of pentacene crystal(2θ=17.7°).

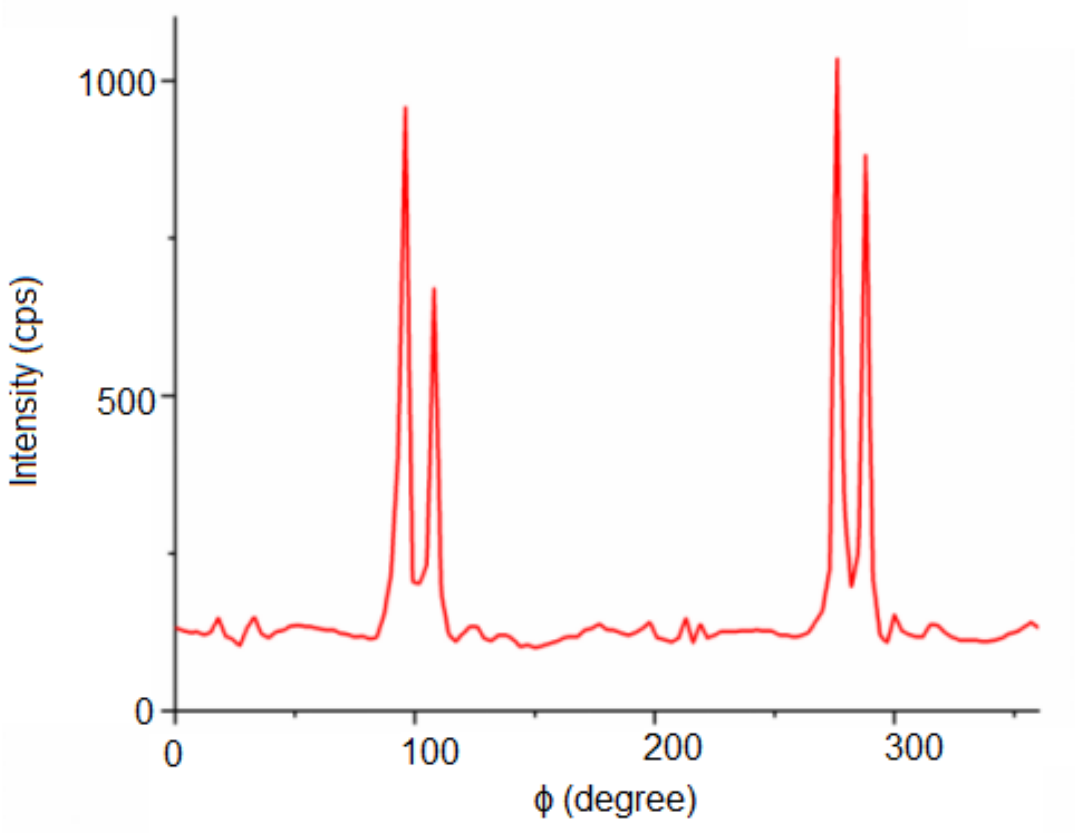

Figure 2-8. ϕ (β) scan of pole figure spot (2θ = 17.7°, α = 16°).

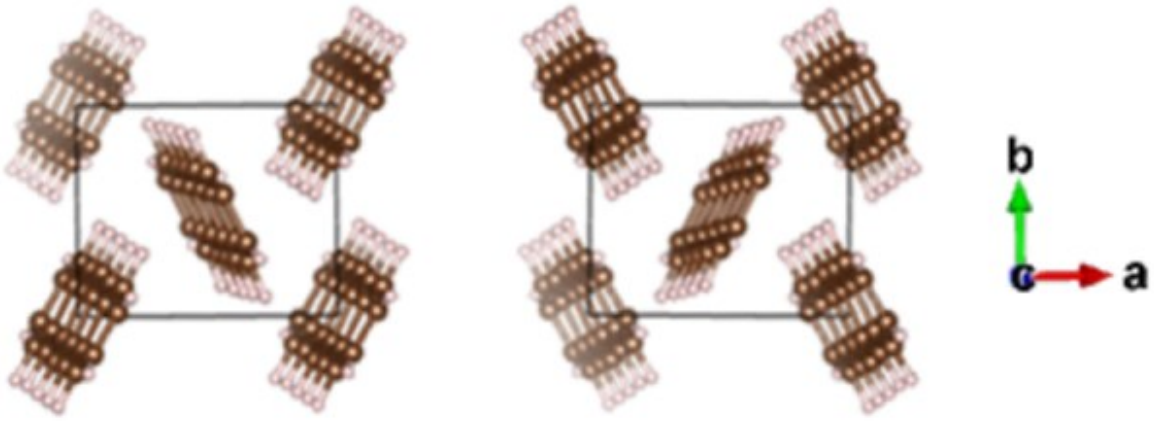

Figure 2-9. Model of the twin structure. [38,45]

Table 1. Unit cell parameters of pentacene "bulk type" (d=14.5Å)

	a (Å)	b (Å)	c (Å)	alpha(°)	beta(°)	gamma(°)
unit cell	7.90	6.06	16.01	101.9	112.6	85.8
reciprocal	0.1371	0.1686	0.06895	78.85	67.77	89.62

Table 2. Unit cell parameters of pentacene "single crystal type" (d=14.1Å)

	a (Å)	b (Å)	c (Å)	alpha(°)	beta(°)	gamma(°)
unit cell	6.265	7.786	14.511	76.65	87.50	84.61
reciprocal	0.1604	0.1325	0.07085	103.18	91.30	94.95

Table 3. Diffraction near 2θ=17.7° of the "bulk type" pentacene

H	K	l	2θ(°)
0	1	1	17.202
0	1	-2	17.3486
1	0	-3	17.7546
1	1	-1	17.8695
0	0	3	18.3389

Table 4. Diffraction near 2θ=17.7° of the "single crystal type" pentacene

H	K	l	2θ(°)
1	0	-1	15.691
1	1	0	17.6364
1	1	1	17.6866
1	0	2	18.7595

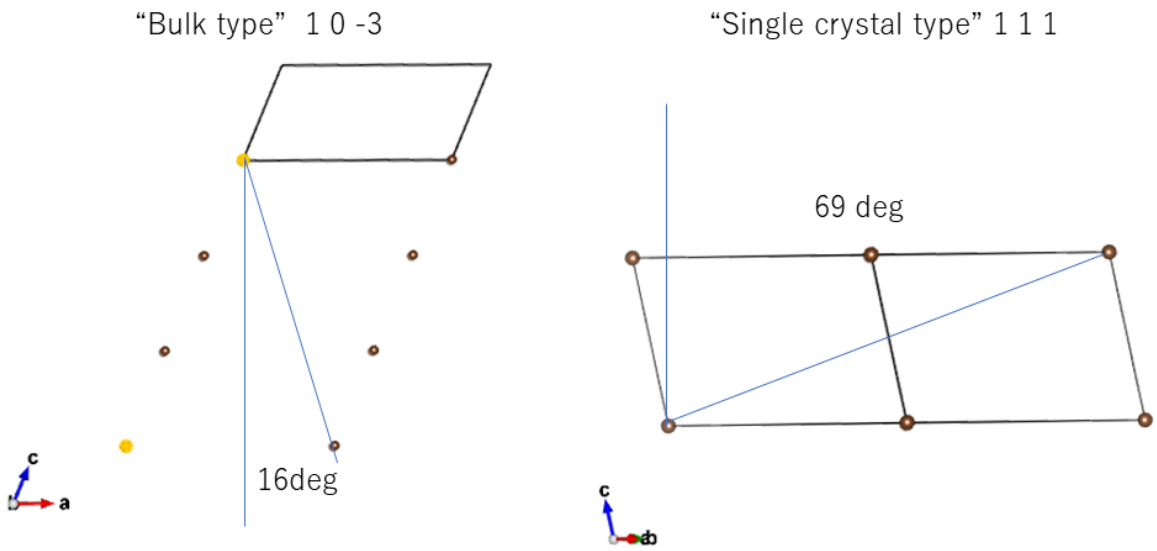

Figure 2-10. Reciprocal lattice calculation for the diffraction near $2\theta = 17.7^{o}$

Finally, I examined the possibility of scaling up the growth apparatus. Although H-shaped glass tubes are good for laboratory scale, it is too time-consuming for the production. I have built an ultrahigh-vacuum compatible stainless steel two-room vessel as shown in Fig. 2-11 (a). By using two zone furnace and a similar temperature profile as described above, I succeeded in the growth of pentacene crystals shown in Fig. 2-11 (b).

Figure 2-11. (a) Scaling up of the growth apparatus. (b) Obtained pentacene crystals.

2.4 Conclusion

In this experiment, I determined the suitable temperature and concentration for pentacene crystal growth from a naphthalene flux solution，the determination of the solubility of pentacene in naphthalene also provides the possibility for pentacene inkjet printing application ：the pentacene ink can be supported at a certain temperature. Through try and error, I successfully established the growth parameter and obtained plate-like crystals of pentacene with almost 1 cm sizes. I analyzed the crystal structure by x-ray diffraction and found that "bulk type" (interlayer spacing 14.5Å) polymorph crystals was formed. The crystals were made of aligned microtwins.

References:

1. S.R. Forrest, *Nature* **2004**, *428*, 911-918.
2. M. Kaltenbrunner, T. Sekitani, J. Reeder, T. Yokota, K. Kuribara, T. Tokuhara, M. Drack, R. Schwodiauer, I. Graz, S. Bauer-Gogonea, S. Bauer, T. Someya, N*ature* **2013**, *499*, 459-463.
3. F. Garnier, R. Hajlaoui, A. Yassar, P. Srivastava, Techniques, *Science* **1994**, *265*, 1684-1686.
4. P. M. Beaujuge, *J. Am. Chem. Soc.* **2011**, *133*,20009-20029.
5. H. Minemawari, T. Yamada, H. Matsui, J. Tsutsumi, S. Haas, R. Chiba, R. Kumai, T. Hasegawa, *Nature* **2011**, *475*, 364-367.
6. Y. Shi, L. Jiang, J. Liu, Z. Tu, Y. Hu, Q. Wu, Y. Yi, E. Gann, C.R. McNeill, H. Li, W. Hu, D. Zhu, H. Sirringhaus, *Nat Commun* **2018,** *9***,** 2933.
7. D.C. Le, D.D. Nguyen, S. Lloyd, T.K. Suzuki, H. Murata, J. Mater. Chem. C. *8* (2020) 14873–14879.
8. Q. Zhang, Front. Phys. 2021, 16, 1, 13602.
9. H. Uoyama, K. Goushi, K. Shizu, H. Nomura, C. Adachi, Nature. 2012, 492, 234–238.
10. H. Matsui, Y. Takeda, S. Tokito, Org. Electron. **2019**, *75*, 105432.
11. H. Jiang, W. Wenping. *Angew. Chem. Int. Ed.* **2020**, *59*, 1408-1428.
12. W. Chen, F. Yu, Q. Xu, G. Zhou, Q. Zhang, *Adv. Sci.* **2022**, *7*, 12, 1903766.

13. T. Minakata, I. Nagoya, M. Ozaki, *J. Appl. Phys*. **1991**, *69*, 7354.

14. R. Ruiz, D. Choudhary, B. Nickel, T. Toccoli, K.-C. Chang, A.C. Mayer, P. Clancy, J. M. Blakely, R. L. Headrick, S. Iannotta, G.G. Malliaras, *Chem. Mater*. **2004**, *16*, 23, 4497-4508.

15. J.Y. Lee, S. Roth, Y.W. Park, *Appl. Phys. Lett*. **2006**, *88*, 252106.

16. D.V. Lang, X. Chi, T. Siegrist, A.M. Sergent, A. P. Ramirez, *Phys. Rev. Lett.* **2004**, *93*, 086802.

17. R.C. Haddon, X. Chi, M. E. Itkis, J. E. Anthony, D. L. Eaton, T. Siegrist, C. Mattheus, T.T.M. Palstra. *J. Phys. Chem. B.* **2002,** *106*, 33, 8288–8292.

18. J. Takeya, C. Goldmann, S. Haas, K.P. Pernstich, B. Ketterer, B. Batlogg, *J. Appl. Phys.* **2003**, *94*, 5800-5804.

19. O.D. Jurchescu, J. Baas, T.T.M. Palstra, *Appl. Phys. Lett.* **2004**, *84*, 3061-3063.

20. M. Kiguchi, M. Nakayama, K. Fujiwara, K. Ueno, T. Shimada, K. Saiki, *Jpn. J. Appl. Phys.* **2003**, *42*, L1408-L1410.

21. D. Guo, T. Miyadera, S. Ikeda, T. Shimada, K. Saiki, *J. Appl. Phys.* **2007**, *102*, 023706.

22. M. Ohtomo, T. Suzuki, T. Shimada, T. Hasegawa, *Appl. Phys. Lett.* **2009**, *95*, 123308.

23. T. Shimada, H. Nogawa, T. Hasegawa, R. Okada, H. Ichikawa, K. Ueno, K. Saiki, *Appl. Phys. Lett.* **2005**, *87*, 061917.

24. H. Fukagawa, H. Yamane, T. Kataoka, S. Kera, M. Nakamura, K. Kudo, N. Ueno, *Phys. Rev. B* **2006**, *73*, 245310.

25. R. Matsubara, N. Ohashi, M. Sakai, K. Kudo, M. Nakamura, *Appl. Phys. Lett.* **2008**, *92*, 242108.

26. N. Sakai, T. Tamura, T. Yanase, T. Nagahama, T. Shimada, *Jpn. J. Appl. Phys.* **2019**, *58*, SBBG08.

27. R.A. Laudise, Ch. Kloc, P. Simpkins, T. Siegrist, *J. Cryst. Growth*, **1998**, *187*, 449-454.

28. S. Arabi, D.J. Atika, M. Mirza, P. Yu, L. Wang, J. He, C. Jiang, *Cryst. Growth Des*. **2016**, *16*, 2624–2630.

29. T. Abe, R. Matsubara, M. Hayakawa, A. Shimoyama, T. Tanaka, A. Tsuji, Y. Takahashi, A. Kubono, *Jpn. J. Appl. Phys.* **2018**, *57*, 03EG13.

30. A. Maliakal, K. Raghavachari, H. Katz, E. Chandross, T. Siegrist, *Chem. Mater.* **2004**, *16*, 4980–4986.

31. K. Sato, T. Sawaguchi, M. Sakata, K. Itaya, *Langmuir.* **2007**, *23*, 12788–12790.

32. Z. Zhang, Q. Zhang, *Mater. Chem. Front.* **2020**, *4*, 3419-3432.

33. Y. Kimura, M. Niwano, N. Ikuma, G. Goushi, K. Itaya, *Langmuir*. **2009**, *25*, 4861–4863.

34. M.A. Wolak, B. Jang, L.C. Palilis, Leonidas, H. Kafafi, *J. Phys. Chem. B*. **2004**, *108*, 5492–5499.

35. Y. Li, Y. Wu, P. Liu, Z. Prostran, S. Gardner, B.S. Ong, *Chem. Mater*. **2007**, *19*, 418-423.

36. I.K. Ahn, W.C. Ghiorse, L.W. Lion, M.L. Shuler, *Biotechnol. Bioeng*. **1998**, *59*, 587-594.

37. H.C. Menezes, B.P. Paulo, N.T. Costa, Z.L. Cardeal, *Microchem. J.* **2013**, *109*, 93-97.

38. T. Siegrist, C. Besnard, S. Haas, M. Schiltz, P. Pattison, D. Chernyshov, B. Batlogg, C.A. Kloc, *Adv. Mater.* **2007**, *19*, 2079-2080.

39. R.B. Campbell, J.M. Robertson, J. Trotter, *Acta. Cryst*. **1961**, *14*, 705.

40. S. Schiefer, M. Huth, A. Dobrinevski, B. Nickel, *J. Am. Chem. Soc*. **2007**, *129*. 10316-10317.

41. C.C. Mattheus, A.B. Dros, J. Baas, G.T. Oostergetel, A. Meetsma, J.L. de Boer, T.T.M. Palstra, *Synthetic Metals* **2003**, *138*, 475-481.

42. T. Siegrist, C. Kloc, J.H. Schön, B. Batlogg, R.C. Haddon, S. Berg, G.A. Thomas, *Angew. Chem. Int. Ed.* **2001**, *40*, 1732-1736.

43. D. Holmes, S. Kumaraswamy, A.J. Matzger, K.P.C. Vollhardt, *Chem. Europ. J.* **1999**, *5*, 3399-3412.

44. A. Troisi, G. Orlandi, *J. Phys. Chem. B.* **2005**, 109, *5*, 1849-1856.

45. K. Momma, F. Izumi, *J. Appl. Crystallography* **2011**, *44*, 1272-1276.

46. D. Guo, K. Sakamoto, K. Miki, S. Ikeda, K. Saiki, *Phys. Rev. Lett*. **2008**, *101*, 236103.

Chapter 3

An anomalous phenomenon of heating C_{60} and naphthalene mixture

3.1 Introduction

Since C_{60} was synthesized by Harold et al. in 1985 [1], it has received extensive attention because of its unique chemical and physical properties and potential application value [2-5]. In recent years, C_{60} has been used in materials science, medicine, electronics, and other fields [6-9]. it has demonstrated the C_{60} application value. Naphthalene is an important hydrocarbon raw material, the melting point of naphthalene is 80.2℃, molten naphthalene provides an excellent solubilizing medium for poorly soluble aromatic compounds [10]. Organic materials with conjugated π bond like OPQP, pentacene etc. have a good solubility in naphthalene [11,12]. As common experience, C_{60} can dissolve in molten naphthalene, but I found an anomalous phenomenon that C_{60} will float on the surface of naphthalene instead of dissolving in it. There is almost no report about this anomalous phenomenon of heating C_{60} and naphthalene mixture.

The aim of this research is to demonstrate this anomalous phenomenon by measuring the change in the vapor pressure of naphthalene by heating different concentrations of C_{60} and naphthalene mixture, in this research I also built different models which contained different numbers of C_{60} molecules in same numbers of neutral naphthalene molecules, the intuitive snapshots of results are given at the microscopic scale in the form of molecular dynamics.

3.2 Materials and Methods

3.2.1 Materials and sample preparation

I first prepared C_{60}-naphthalene samples. C_{60} and naphthalene mixtures were added in the quartz tubes, then all the samples were vacuum sealed. Figure 3-1 shows the schematic of naphthalene vapor concentration measurement device, the light source was on the right side (XENON LAMP POWER SUPPLY), the sealed sample was placed in a temperature-controlled aluminum block which contained 4 heaters inside, the temperature of the aluminum block was controlled by two heaters on the upper and lower sides, respectively. There is a hole in the medium of the aluminum block which allowed the light passes through, the amount of added C_{60} was controlled to make sure that the light can pass through the blank part of the quartz tube rather than passing through the molten/melt naphthalene solution. Between the light source and aluminum block there is a monochromator (Jasco CT-10), adjusted the wavelength of the light to 270nm which agree with the naphthalene excitation wavelength [13], finally the transmitted light reached to the photo multiplier (Keithley). Heating the aluminum block, the naphthalene will be gradually melting, light intensity will decrease as the blank part of quartz tube gradually increasing with the concentration of naphthalene vapor. In this research, I prepared samples with different weight percentages which were 0.174, 0.467, 0.685 and 0.902 wt%, respectively. The amount of naphthalene in each sample is controlled at about 0.08g to make sure that the concentration of naphthalene vapor will not be affected by the

amount of naphthalene.

The naphthalene vapor concentration is calculated based on the Lambert-Beer`s law:

$$\log_{10}(I_0/I) = \varepsilon bc \qquad (1)$$

Where I_0 and I are the incident light intensity and the transmitted light intensity, respectively. ε is the molar absorption coefficient, b is the light path, and c is the concentration of naphthalene vapor.

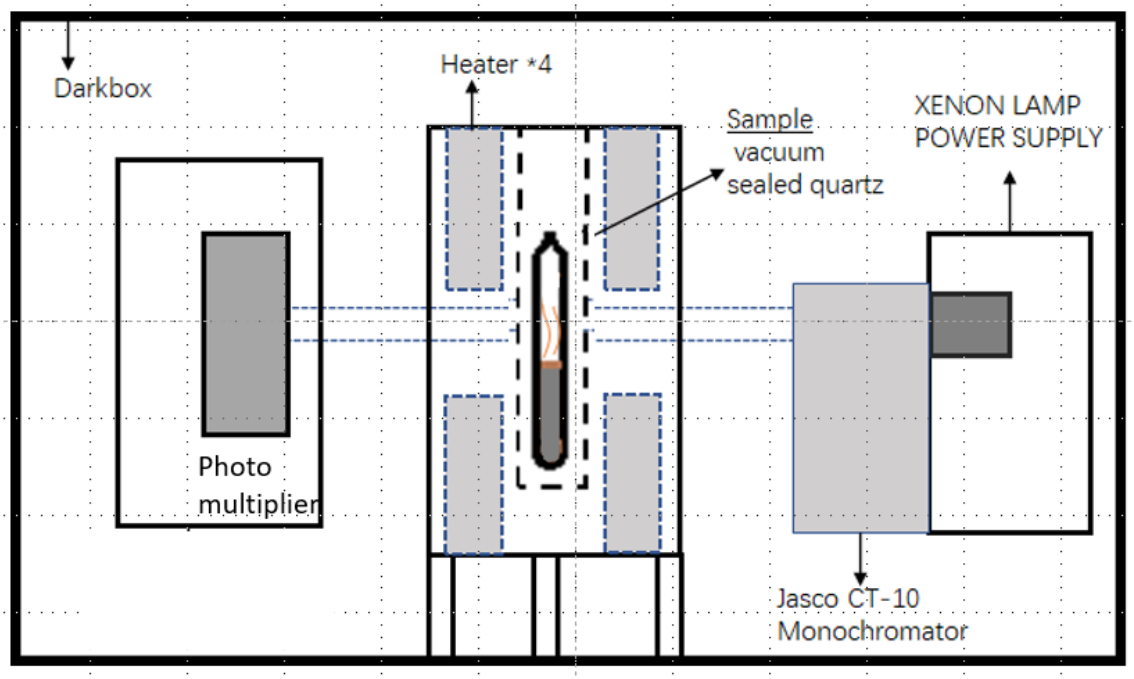

Figure 3-1 Schematic of naphthalene vapor concentration measurement device.

3.2.2 Simulation details

The naphthalene and C_{60} mixture models were designed by Packmol and moltemplate software [14,15], 670 neutral naphthalene molecules were used as solvent, C_{60} molecules were used as solute, Gaussian 16 [16] calculation of single molecules of naphthalene had given 0.05 electron and C_{60} had given -0.05 electron charge transfer, the same numbers

of charged naphthalene as C_{60} were introduced to keep the charge neutrality of the system. Figure 3-2 shows the 670 neutral naphthalene molecules with 15-15, 30-30 and 100-100 charged naphthalene and C_{60} molecules models, respectively.

All simulations were performed by the MD software package LAMMPS [17]. In LAMMPS the motion equations are based on the work of Shinoda et al., Martyna et al., and Parrinello et al [18-20]. All molecules were parameterized using LigParGen with OPLS-AA force field [21-23]. A 70 Å *70 Å *70 Å simulation box with periodic boundaries was applied on all simulations, I used the cutoff distance rcut =11 Angstrom for all simulations.

First simulation was carried out for the naphthalene and C_{60} mixture model in the isobaric-isothermal (NPT) ensembles at 0 atmospheric for 100 fs, temperature raised up from 2.5 to 300K. Then in the NPT ensembles for 6 fs to relaxation at the 300K, 0 atmospheric. A Nose-Hoover temperature thermostat and Nose – Hoover pressure barostat [24,25] were used in all NPT ensembles. Finally, the mixture model was in the canonical ensemble (NVT) at 300 K, 0 atmospheric for 200000 fs, both Nose – Hoover and Langevin thermostats [26] were used in NVT ensemble. For all simulations real atomic masses were used.

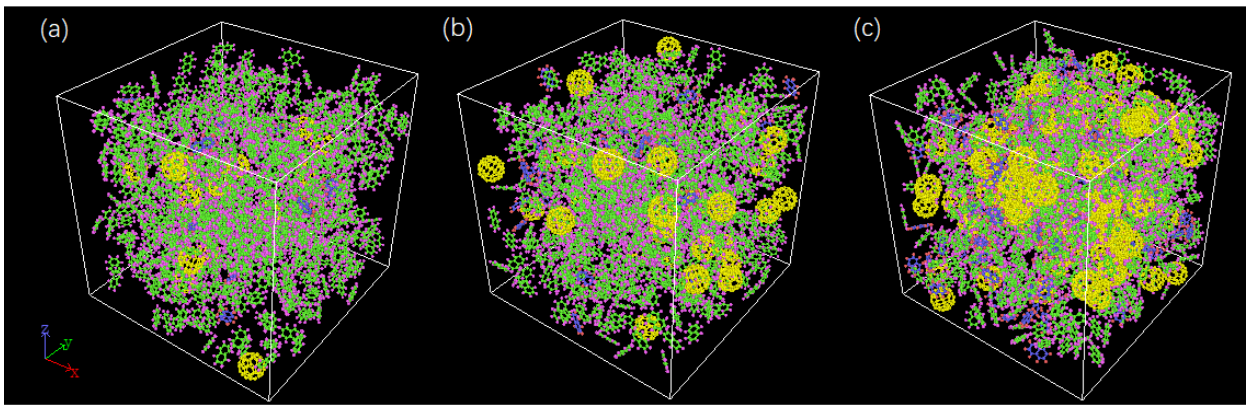

Figure 3-2 Green-purple molecules are the neutral naphthalene molecules, blue-red molecules are the charged molecules, yellow molecules are the charged C_{60} molecules. From left to right, Figure 3-2(a) 15 charged C_{60}; 15 charged naphthalene and 670 neutral naphthalene molecules model. 2(b) 30 charged C_{60}; 30 charged naphthalene and 670 neutral naphthalene molecules model. 2(c) 100 charged C_{60}; 100 charged naphthalene and 670 neutral naphthalene molecules model.

3.3 Results and discussions

3.3.1 Experiment results

The incident light intensity I_0 was obtained by measuring a vacuum sealed quartz tube, the heating temperature is from room temperature to 260 ℃, the light intensity data was recorded per 10 ℃, the light intensity value changed from 7.27 to 7.31, here the average value 7.28 is used as I_0 value. Then 5 different concentrations of C_{60} in naphthalene samples were measured, when temperature below 110℃ naphthalene is a solid state which has no great influence on the blank part of the quartz tube to be tested, all samples

were almost agree with vacuum sample. If we assume the ε as a coefficient, the concentration c can be calculated by equation (1). Here, Figure 3-3 I show optical absorbance of 5 different concentrations samples at 270nm from room temperature to 260 ℃, the black curve shows naphthalene vapor concentration which the sample only contained naphthalene, the red, blue, purple, and green curves represent 0.174, 0.467, 0.685 and 0.902 wt% C_{60}-naphthalene samples, respectively. As the concentration of C_{60} increasing, the vapor concentration of naphthalene showed an obvious decreasing, in other words, the higher the concentration of C_{60}, the stronger the evaporation inhibition of naphthalene vaporization.

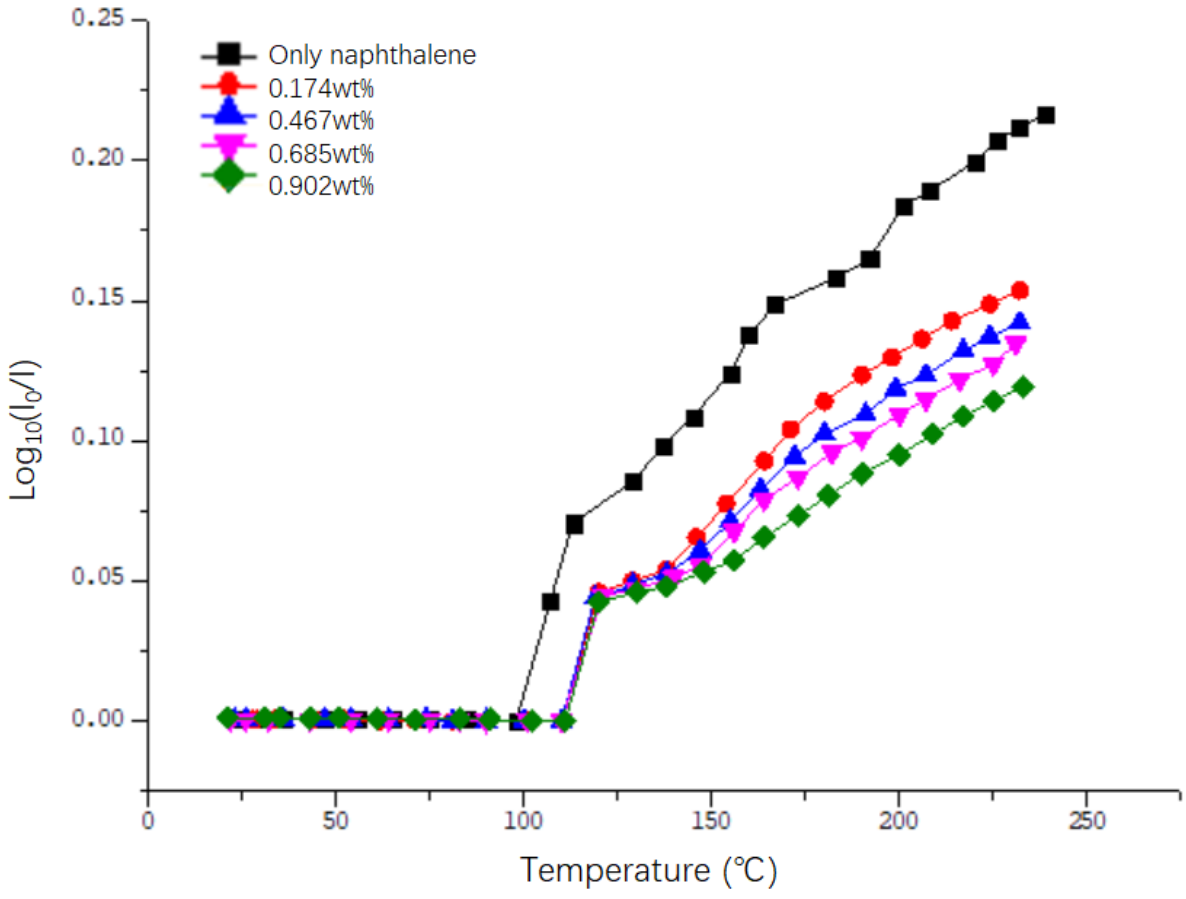

Figure 3-3 Naphthalene vapor concentration-temperature dependence curves of C_{60} and naphthalene mixture.

3.3.2 Controlled experiment results

Here I measured pentacene and naphthalene mixture as controlled experiment. Two samples were prepared which the concentrations were 0.509 and 0.617 wt%, respectively. Light intensity data was recorded per 10℃, the amount of naphthalene in each sample was about 0.08g. After calculating by equation (1), the obtained results are shown in Figure 3-4, the black curve represents the sample only contained naphthalene, the curve is same as the result of the sample only contained naphthalene in Figure 3-3, the red and blue curves represent 0.509wt% and 0.617wt%, respectively. The curves are approximately same even though the concentrations of pentacene and naphthalene mixture are different, pentacene did not exhibit the same inhibition of naphthalene vaporization as C_{60} samples.

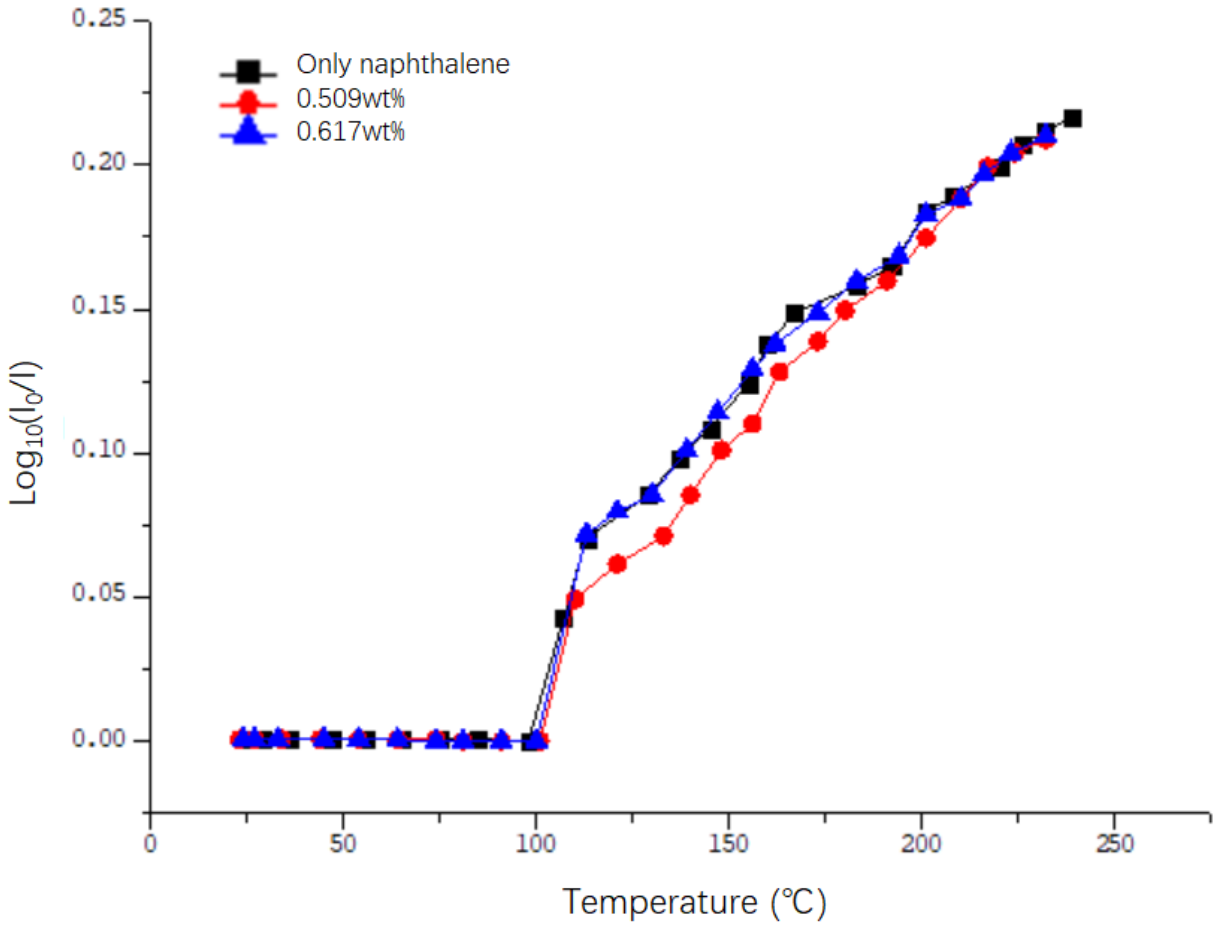

Figure 3-4 Naphthalene vapor concentration-temperature dependence curves of pentacene and naphthalene mixture.

Here, a summarize of the experiment results are shown in Figure 3-5. At about 100℃, naphthalene vapor can be It can be seen that C_{60} has a significant inhibitory effect on the vaporization of naphthalene, the reason may be because C_{60} floats on the surface of naphthalene, forming clusters or layers, like a cover blocked the naphthalene vapor.

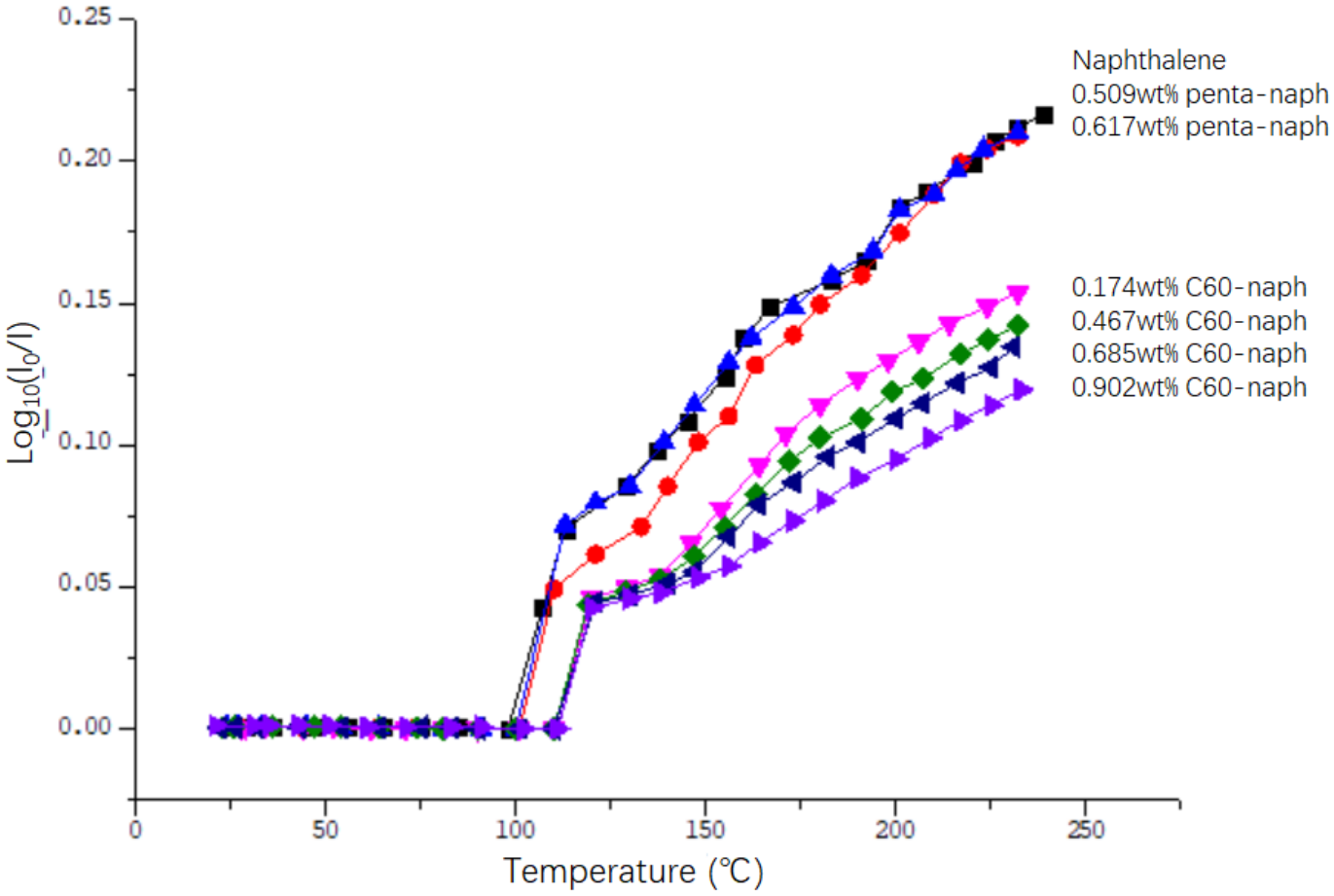

Figure 3-5 A summarize of the C_{60}-naphthalene mixture and pentacene-naphthalene mixture samples measurement results.

3.3.3 Simulation results

Figure 3-6 I take 30 charged naphthalene, 30 charged C_{60} and 670 neutral naphthalene molecules as simulation example. The left figure shows a snapshot of the initial structure of the mixture at 0 fs, 0K, the charged naphthalene, charged C_{60} and neutral naphthalene molecules were well mixed, then after 100fs, the system temperature reached to 300K which enough for naphthalene melting, naphthalene molecules shrined and tended to form

a cluster, whether charged or neutral naphthalene molecules. At same time C_{60} also had a tendency to be expelled out of the naphthalene cluster, in the middle figure, the C_{60} molecules that were mixed inside the model in the initial structure are now floating on the surface of the naphthalene cluster. Right figure shows a snapshot of mixture model which had relaxation for 200000fs at 300K in the NVT ensemble, both neutral and charged naphthalene molecules were gathering and formed a cluster, C_{60} molecules were expelled out from the naphthalene cluster and floated on the surface of the naphthalene.

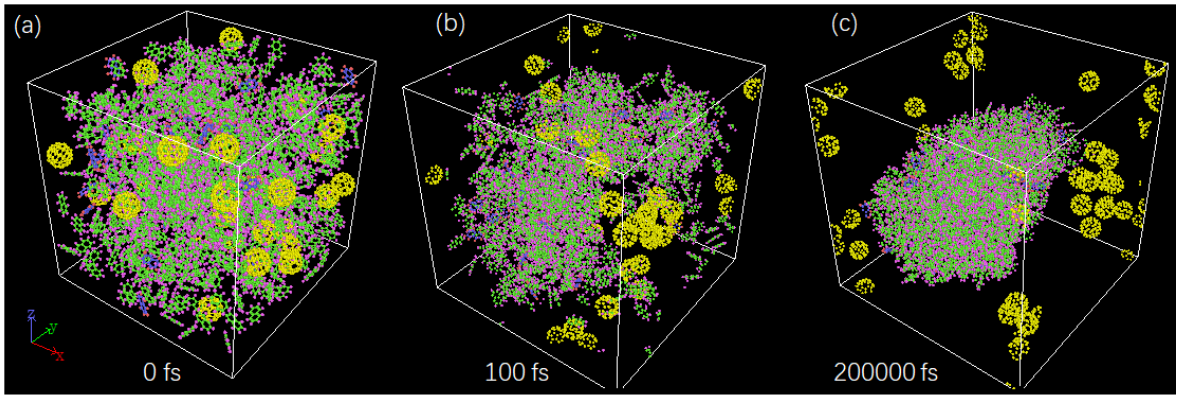

Figure 3-6 30 charged C_{60} and 30 charged naphthalene molecules in 670 naphthalene molecules model, the snapshots of simulation results: (a) 0 fs, initial structure; (b) 100 fs, 300K melting state; and (c) 200000 fs, NVT relaxation at 300 K.

Considering the reason of the repulsive force generated after C_{60} forms clusters, different numbers of C_{60} molecular models were constructed. Except for the different number of C_{60} molecules, other three groups of simulations were carried out under the same simulation conditions. Figure 3-7 shows the simulation results of different numbers of charged C_{60} and charged naphthalene molecules in 670 neutral naphthalene molecules, the 670 neutral naphthalene molecules result was also included. Figure 3-7 (a): after

temperature reached to 300K, in the NVT ensemble at 200000 fs, the snapshots of only 670 neutral naphthalene molecules; (b): 15 charged C_{60}, 15 charged naphthalene and 670 neutral naphthalene molecules; (c): 100 charged C_{60}, 100 charged naphthalene and 670 neutral naphthalene molecules, respectively. Compare with the model which only contained naphthalene molecules, even with only 15 C_{60} molecules model shows a certain phenomenon that C_{60} molecules were expelled out from the naphthalene. The addition of C_{60} molecules also seems to have an impact on the shape of the naphthalene clusters at equilibrium state. This may be due to the large repulsive force of C_{60} clusters.

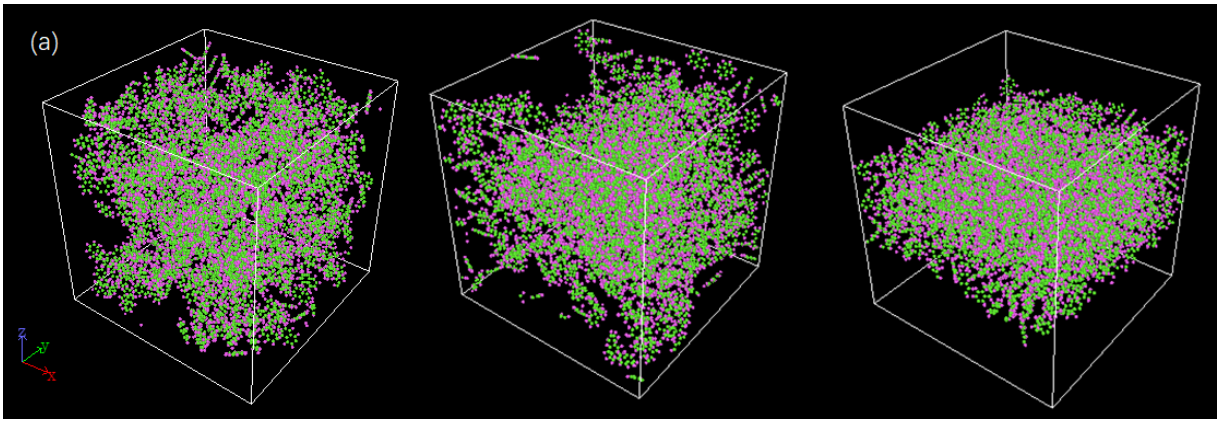

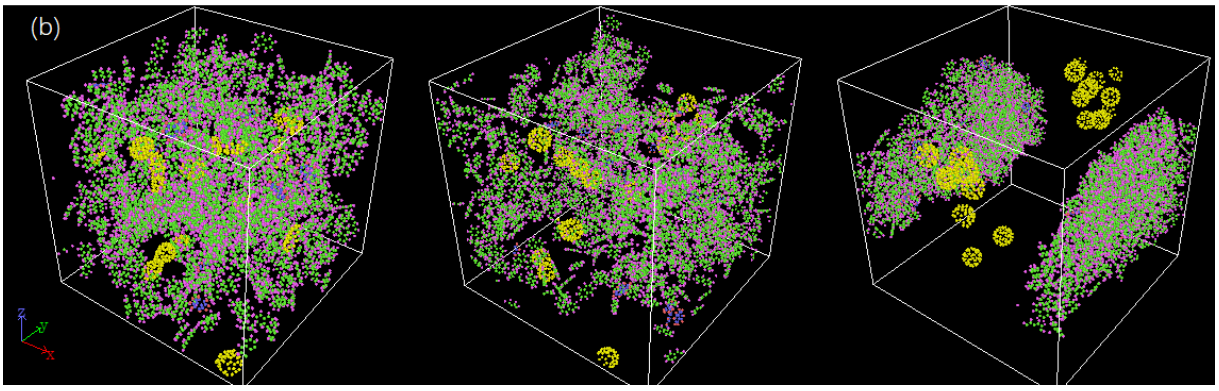

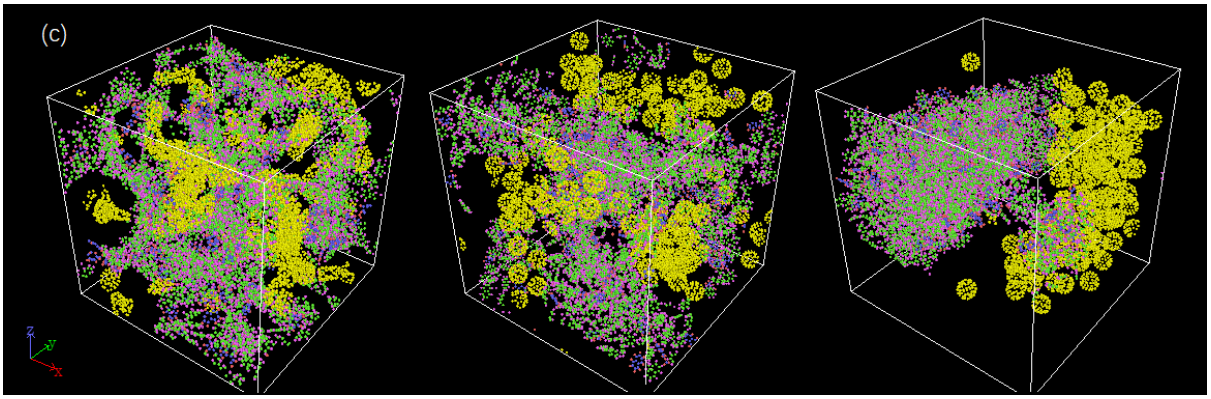

Figure 3-7 Snapshots of different models, temperature from 0K to 300K in NPT ensemble and relaxation in NVT ensemble for 200000 fs (300K) results. (a) 670 neutral naphthalene. (b) 15 charged naphthalene, 15 charged C_{60} and 670 neutral naphthalene. (c) 100 charged naphthalene, 100 charged C_{60} and 670 neutral naphthalene.

3.3.4 Controlled simulation results

Pentacene and naphthalene mixture model was simulated as a controlled simulation, the pink-yellow molecules are the pentacene molecules. Pentacene molecules contained hydrogen atoms, the parameters related to hydrogen in the simulated force field, except this, the other simulation conditions were same as C_{60}-naphthalene simulations. The snapshots of pentacene-naphthalene simulation results can be found in figure 3-8, from left to right shows: (a) 0 fs, at 0k, the initial mixture model, which contained 30 charged pentacene, 30 charged naphthalene and 670 neutral naphthalene, all the molecules were mixed; (b) at 100 fs, 300k, the mixture system temperature reached to 300K, an increase in temperature causes all molecules to start moving; (c) at 200000 fs, 300k, mixture model relaxation in the NVT ensemble, it can be seen that the pentacene molecules were not

separated from the naphthalene molecules, compared with figure 3-7(a), the shape of the naphthalene molecular clusters was also not affected by the pentacene molecules. The anomalous behavior as C_{60} in naphthalene was not found in the controlled simulation results.

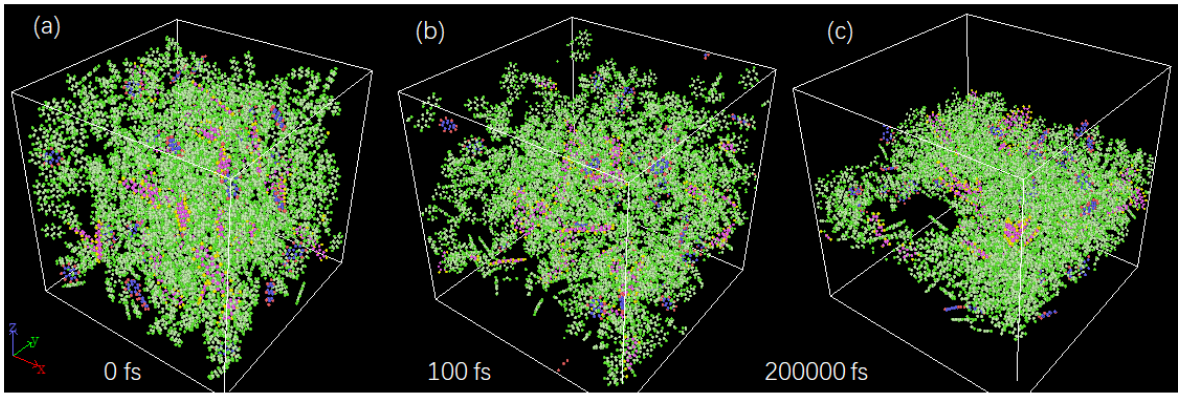

Figure 3-8 30 charged pentacene and 30 charged naphthalene molecules in 670 naphthalene molecules model as a controlled simulation, (a) at 0 fs, initial structure. (b) at 100 fs, melting state at 300K. (c) at 200000 fs, after NVT relaxation at 300K.

The simulation results show that during the heating process, C_{60} molecules will be expelled out from the naphthalene molecules and floated on the surface of naphthalene instead of dissolving in naphthalene, combine with the simulation results, our experimental results can be explained: when the temperature raised up, C_{60} will be expelled out and float on the naphthalene surface, then the vapor of naphthalene will be blocked by the C_{60}, the higher the concentration of C_{60}, the more obvious the inhibition of naphthalene vaporization. The simulation results show that C_{60} molecules formed a cluster the reason is due to the strong intermolecular interactions between C_{60} molecules[27-30]. In the earlier day`s research, Rodney S. Ruoff, et al. reported an

anomalous solubility of C_{60} in organic solvents (hexane and CS_2)[31] that is at room temperature the solubility of C_{60} have max value, then the solubility decreases with the temperature increases. The author explained this anomalous solubility maybe due to the phase change in solid C_{60}, presumably the phase change observed previously in the absence of a solvent, modified by solvent wetting. This work, the anomalous phenomenon may have the same reason as the reported one, but still need further research to understand the mechanics. I should admire that the principle of this work, the anomalous phenomenon of heating C_{60} and naphthalene was not understood so far, there are several factors may cause this phenomenon, like van der Waals interactions between C_{60} -C_{60} pairs, C_{60} -naphthalene, even naphthalene-naphthalene, or the solvation shell phenomenon may also have impact on this phenomenon, but this work may provide a possibility for the further research, this phenomenon maybe applied on the suppression of toxic solvents vaporization.

3.4 Conclusion

In this research I found an anomalous phenomenon of heating C_{60} and naphthalene mixture and verified through both experimental and simulation methods, while raising the temperature of the C_{60} and naphthalene mixture from room temperature to about 230℃, at about 100℃, the C_{60} will be gradually expelled out of naphthalene and floats on its surface, instead of dissolving in it which shows a strong inhibition of naphthalene vapor. The higher concentration of C_{60}, the more obvious this inhibitory effect is. This

phenomenon maybe due to the phase change on solid C_{60} which were modified by molten/melt naphthalene during the heating process. This anomalous phenomenon was also demonstrated by simulation results, C_{60} molecules were gradually expelled out from naphthalene molecules as the temperature increases, at 300K, the C_{60} molecules completely separated from the mixture. this work may provide a possibility for the further research, I should admire that the principle of this phenomenon was not understood so far, but this work may provide a possibility for the further research, this phenomenon maybe applied on the suppression of toxic solvents vaporization.

References:

1. Kroto, H.W., Heath, J.R., O'Brien, R.F.C., Smalley, R.E. *Nature* **1985**, 318, 162–163.
2. Wudl F. *Journal of Materials Chemistry*, **2002**, 12, 7, 1959-1963.
3. Pan Y, Liu X, Zhang, W., Liu, Zhifeng., Zeng, Guangming., Shao, Binbin., Liang, Qinghua., He, Qingyun., Yuan, Xingzhong., Huang, Danlian., Chen, Ming. *Applied Catalysis B: Environmental,* **2020**, 265: 118579.
4. Afreen, S., Muthoosamy, K., Manickam, S., Manickam, S., Hashim, U. *Biosensors and Bioelectronics,* **2015**, 63, 354-364.
5. Imahori, H., Sakata, Y. *Advanced Materials,* **1997**, 9, 7, 537-546.
6. Sabirov, D.S. *The Journal of Physical Chemistry C*, **2013**, 117, 2, 1178-1182.
7. Ali, S.S., Hardt, J.I., Quick, K.L., Kim-Han, J.S., Erlanger, B.F., Huang, T.T., Epstein, C.J., Dugan, L.L. *Free Radical Biology and Medicine,* **2004**, 37, 8, 1191-1202.
8. Palstra, T.T.M., Zhou, O., Iwasa, Y., Sulewski, P.E., Fleming, R.M., Zegarski, B.R. *Solid state communications,* **1995**, 93, 4, 327-330.
9. Haddon, R.C. *Accounts of chemical research,* **1992**, 25, 3, 127-133.
10. Naphthalene In Wikipedia, The Free Encyclopedia. Available online: https://en.wikipedia.org/w/index.php?title=Naphthalene&oldid=1106859105 (19, October **2022**)

11. Yanase, T., Tanoguchi, H., Sakai, N., Jin, M., Yamane, I., Kato, M., Ito, H., Nagahama, T., Shimada, *Crystal Growth & Design*, **2021**, 21, 8, 4683-4689.
12. Sakai, N., Tamura, T., Yanase, T., Nagahama, T., Shimada, *Japanese Journal of Applied Physics,* **2019**, 58, SBBG08.
13. Dixon, J.M., Taniguchi, M., Lindsey, J.S. *Photochemistry and photobiology,* **2005**, 81, 1, 212-213.
14. Martínez, L., Andrade, R., Birgin, E.G., Martínez, J.M. *Journal of Computational Chemistry,* **2009**, 30, 13, pp 2157-2164.
15. Jewett, A.I., Stelter, D., Lambert, J., Saladi, S.M., Roscioni, O.M., Ricci, M., Autin, L., Maritan, M., Bashusqeh, S.M., Keyes, T., Dame, R.T., Shea, J-E., Jensen, G.J., Goodsell, D.S. *J. Mol. Biol.* **2021**, 433, 11, 166841.
16. Frisch, M.J., Trucks, G.W., Schlegel, H.B., Scuseria, G.E., Robb, M.A., Cheeseman, J.R., Scalmani, G., Barone, V., Petersson, G.A., Nakatsuji, H., Li, X., Caricato, M., Marenich, A.V., Bloino, J., Janesko, B.G., Gomperts, R., Mennucci, B., Hratchian, H.P., Ortiz, J.V., Izmaylov, A.F., Sonnenberg, J.L., Williams-Young, D., Ding, F., Lipparini, F., Egidi, F., Goings, J., Peng, B., Petrone, A., Henderson, T., Ranasinghe, D., Zakrzewski, V.G., Gao, J., Rega, N., Zheng, G., Liang, W., Hada, M., Ehara, M., Toyota, K., Fukuda, R., Hasegawa, J., Ishida, M., Nakajima, T., Honda, Y., Kitao, O., Nakai, H., Vreven, T., Throssell, K., J.A, M.Jr.; Peralta, J.E., Ogliaro, F., Bearpark, M.J., Heyd, J. J., Brothers, E.N., Kudin, K.N., Staroverov, V.N., Keith, T.A., Kobayashi, R., Normand, J., Raghavachari, K.,

Rendell, A.P., Burant, J.C., Iyengar, S.S., Tomasi, J., Cossi, M., Millam, J. M., Klene, M., Adamo, C., Cammi, R., Ochterski, J.W., Martin, R.L., Morokuma, K., Farkas, O., Foresman, J.B., Fox, D.J. Gaussian 16, Revision A.03, Gaussian, Inc., Wallingford CT, **2016**.

17. Thompson, A.P., Aktulga, H.M., Berger, R., Bolintineanu, D.S., Brown, W.M., Crozier, P.S., in 't Veld, P.J., Kohlmeyer, A., Moore, S.G., Nguyen, T.D., Shan, R., Stevens, M.J., Tranchida, J., Trott, C., Plimpton, S.J. *Comp Phys Comm,* **2022**, 271, 10817.
18. Shinoda, W., Shiga, M., Mikami, M. *Phys. Rev.B,* **2004**, 69, 134103.
19. Martyna, G.J., Tobias, D.J., Klein, M.L. *J. Chem. Phys.* **1994**, 101, 4177.
20. Parrinello, M., Rahman, *J. Appl. Phys.* **1981**, 52, 7182.
21. Jorgensen, W.L., Tirado-Rives, J. *Proceeding of the National Academy of Science.* **2005**, 102, 19, 6665-6670.
22. Dodda, L.S., Vilseck, J.Z., Tirado-Rives, J., Jorgensen, W.L. *J. Phys. Chem. B,* **2017**, 121, 15, pp 3864-3870.
23. Dodda, L.S., Cabeza de Vaca, I., Tirado-Rives, J., Jorgensen, W. L. *Nucleic Acids Research,* **2017**, 45, 3, W331-W336.
24. Hoover, W.G. *Phys. Rev. A,* **1985**, 31, 1695.
25. Hoover, W.G. *Phys. Rev. A,* **1986**, 34, 2499.
26. Schneider, T., Stoll, E. *Phys. Rev. B,* **1987**, 17, 1302.
27. Bokare, A.D., Patnaik, A. *The Journal of Physical Chemistry B,* **2005**, 109, 1, 87-

92.

28. Hungerbühle, H. R.; Guldi, D. M.; Asmus, K. D. *J. Am. Chem. Soc.* **1993**, 115, 3386.

29. Bensasson, R. V.; Bienvenue, E.; Dellinger, M.; Seta, S. J. *J. Phys. Chem.* **1994**, 98, 3492−3500.

30. Janot, J. M.; Bienvenue, E.; Seta P.; Bensasson, R. V.; Tome, A. C.; Enes, R. F.; Cavaleiro, J. A. S.; Camps, S. X.; Hirsch, A. J. *Chem. Soc., Perkin Trans.* **2000**, 22, 301−306.

31. Ruoff, R.S., Malhotra, R., Huestis, D.L., Tse, D.S., Lorents, D.C. *Nature,* **1993**, 362, 6416, 140-141.

Chapter 4

Molecular dynamics simulation of poly (ether ether ketone) (PEEK) polymer to analyze intermolecular ordering by low wavenumber Raman spectroscopy and x-ray diffraction

4.1 Introduction

Poly (ether ether ketone) (PEEK) is a high-performance thermoplastic and crystal-line polymer with excellent mechanical properties, inertness in harsh chemical environment, and thermal durability [1-3]. Reinforced composite materials of the PEEK with inorganic or carbon fiber fillers have attracted attention as a structural material for aircraft and automobiles because of the light weight and excellent properties. It is established that the degree of crystallinity greatly affects mechanical properties of crystalline polymers including PEEK. Since it has been reported that the crystallinity of fiber reinforced polymers may be spatially non-uniform [4,5], it is important to evaluate local crystallinity less than the diameter of the filler fibers. Since the size of the fiber fillers are on a scale of several μm, evaluation of crystallinity in sub-μm region is important. There are various techniques for the evaluation of crystallinity of polymers such as wide-angle X-ray diffraction (WAXRD), Small-angle X-ray diffraction (SAXS), differential scanning calorimetry (DSC), Fourier transform infrared (FTIR) spectroscopy and Raman microscopy [6,7]. Among them, Raman microscopy that takes Raman spectra under the focus of an objective lens, is probably the only readily available technique [8]. X-ray diffraction microscopy using synchrotron light source[9] or cryogenic transmission electron microscopy [10] are now possible, but the location and machine time for the measurement are very limited and the preparation of the samples in very thin slabs shape is troublesome. Raman microscopy can be measured in the reflection geometry with the

high resolution of optical microscopy that can easily reach sub-μm and possible to measure the local vibrational spectrum.

There are several reports on the application of Raman spectra for the evaluation of crystallinity of PEEK [6,7,11-15]. Usually, the frequency shift of fundamental vibration modes involving a single or several covalent chemical bonds (intramolecular modes) are used to characterize the crystallinity. However, the shift of the intramolecular modes comes from the difference in the local environment surrounding the chemical bonds, and it does not reflect the crystallinity in straightforward fashion. Since there are "intermolecular modes" in molecular materials including polymers, which resides in low frequency [16-18]. Intermolecular modes are expected to be more sensitive to the crystallinity, because the intermolecular distances and angles, and chain alignment in polymers will be affected by the crystallinity. A team including some of the present authors has reported the use of low frequency Raman signal to evaluate the crystallinity of PEEK [7]. Although they found that the intensity of a Raman signal changes during the crystallization as explained in the next section, the mechanism has not been elucidated. The aim of this paper is to understand the mechanism from molecular dynamics simulation (MD) with a new analysis scheme.

Molecular vibration of a single molecule can be calculated by first principle calculation using the real space basis functions, and phonons in a crystal can be calculated by the analysis in the reciprocal space. Intermolecular phonons in crystalline polymers are difficult to analyze from both of the above-mentioned approach. Infinitely large ideal

polymer crystals cannot be treated purely in the real space, and too much degree of the freedom in the unit cell hinders ordinary calculation techniques in the reciprocal space. Another problem is the connection between vibration modes with Raman spectroscopy. In the Raman spectroscopy, temporal oscillation of local polarizability due to the molecular vibration makes the scattering of incoming photons with loss or gain of the phonon energy. Calculation of polarizability requires quantitative evaluation of the electronic structure of the material and its change caused by the vibration. Although it has become possible to calculate intermolecular vibrational modes of polymer crystals from first principles [17,18], it is computationally very heavy to be applied to the large inhomogeneous system including the polymer composites.

In this paper, I present a computationally alleviated approach using classical MD. MD can track the motion of each atom under various conditions, such as constant temperature, pressure, volume, energy etc. The information of the chemical bonding and intermolecular interaction is contained in the force field (FF) in the classical MD. There are various types of FF and the parameters have been determined by various experimental physical properties such as melting points and heat of phase transitions, and some of them use the result of quantum chemical calculations. They are still im-proved by using first-principle calculations combined with data science approach. If the MD is performed long enough time and the atomic motion is "Fourier-transformed", it should contain the information of molecular / lattice vibrations. It will be a reason-able alternative for the molecular vibration analysis if the atomic motion can be related to the

spectroscopy such as Raman spectroscopy. Here propose an approximation of the local polarizability by approximated valence electron densities that will be explained in the Materials and Method section. Fast Fourier transform (FFT) of the time variation of the local polarizability is used to derive data corresponding to Raman spectra. Intramolecular vibration is evaluated by DFT quantum chemical calculation.

The MD can be used to simulate x-ray diffraction also, which is more straight-forward than the vibrational analysis and implemented in many software packages. I use it to compare the experimental wide angle x-ray diffraction (WAXRD).

4.2 Materials and Methods

4.2.1 Extraction of approximate Raman signal from MD simulation

The probability of Raman scattering is described by the Raman polarizability tensor, which is simplified by Placzek approximation [19,20] to eq.(1):

$$(\alpha_{\alpha\beta})_{\nu m \nu n} = \frac{2}{\hbar}\sum_{j\neq n} \frac{\omega_{jn}}{\omega_{jn}^2-\omega^2}\langle \nu m|Re\langle n|\mu_\alpha|j\rangle\langle j|\mu_\beta|n\rangle|\nu n\rangle$$

in the case of Stokes Raman scattering. Here, the lefthand side of the equation is the Raman polarizability tensor corresponding to the vibrational transition from νn to νm, n and j denote the ground state of electrons and excited states, respectively. ω_{jn} is the energy difference between state *n* and *j* in angular frequency and ω the angular frequency of the incoming electromagnetic wave. μ_α and μ_β are dipole moment operators in the direction of α and β.

Calculation of this quantity requires the calculation of precise electronic states of the

molecule and its dependence on the position of the nuclei vibrating from the ground state. It becomes computationally very demanding in the case of polymer aggregates because of the many degrees of structural freedom as mentioned in the Introduction. Also, accurate treatment of van der Waals interaction becomes computationally very demanding but necessary for the estimation of intermolecular vibration. Our approach proposed here is to use an approximate local valence electron density. The motion of valence electrons by the external electric field is the cause of the dynamic dipole moment associated with the transition $\langle n|\ \mu_\alpha\ |j\rangle$ and $\langle j|\ \mu_\beta\ |n\rangle$. The fluctuation of the local valence electron density at the frequency of a vibration mode vm can be assumed proportional to them. Therefore, we can approximate the Raman intensity at vibrational frequency ν as proportional to the squared oscillation of valence electron density ρ caused by vibration:

$$(\alpha_{\alpha\beta})_{vmvn} \propto \rho^2(\nu) \qquad (2)$$

Since it is established that Raman scattering can occur in a single molecule [22], I can justify a crude approximation to neglect the spatial phase of the electric field of the incoming photons and consider the scattering locally at the position x in the material:

$$(\alpha_{\alpha\beta})_{vmvn} \propto \int \rho^2(x,\nu)\, dx \qquad (3)$$

There will be various ways to calculate the local valence electron density. In this paper, I use a very simple approximation as follows:

$$\rho(x) = \sum_i N_i \exp\left(-\frac{|\ x - r_i\ |}{R_i}\right), \qquad (4)$$

where ρ (x) is the valence electron density at the position x, N_i and R_i are the valence electron number and characteristic atom radius of atom i, respectively. r_i is the position

of the atom i. Here I used values for N_i the nominal valence electron count of each atom (C 4, O 6, H 1) and for Ri covalent radius (C 0.73Å, O 0.66Å, H 0.32Å) [23]. In the following, I show the Fourier transform of ρ, not ρ^2, to enhance the small features.

This type of simplification of molecules is recently used in machine learning for protein engineering and has been proved to work to extract microchemical environment of biological polymers [24,25].

4.2.2 Computation details

Molecular vibrations of single strand PEEK oligomers were calculated by DFT calculation using Gaussian16 [26] at B3LYP/6-31G level of theory. The MD simulation was performed using LAMMPS [27] with generalized AMBER FF(GAFF) [28]. The atomic charges for the calculation of Coulomb interaction was calculated by Gaussian16 of a PEEK oligomer at B3LYP/6-31G level. The initial structure of the polymer based on the reported crystal structure [29] was prepared by moltemplate utility [30]. There are several crystal structure parameters for PEEK [31-38] but they agree with each other only with small deviation of the lattice constant and atom positions [6]. The results were visualized by OVITO [39] and VESTA [40]. The atomic trajectory data, including Fourier transform and smoothing spline fitting were analyzed using home-made programs written with python 3.7. The vibration mode at frequency ν (Hz) is expressed in the unit of wavenumber $\tilde{\nu}$ (cm^{-1}) throughout this paper using

$$\tilde{\nu} = \nu / c , \qquad (5)$$

where c is the light speed.

4.2.3 Experiments

To compare the calculation with the expements, WAXRD patterns and Raman spectra were measured on the samples annealed at various temperatures up to 300 oC for 2h. The sample material was a quenched PEEK thin film with the thickness of 50mm (Victrex APTIV film, grade 1000). The detail of the experiment is described in [7]. WAXRD was measured by using Rigaku Ultima IV (rotating anode, 40kV 30mA) oper-ating with CuKa x-ray (wavelength 1.5406 Å. Raman spectroscopy was measured using Horiba Jobin Yvon LablamHR spectrometer with Nd:YAG laser (wavelength 1064 nm, spot size 1 μm) with × 50 magnification microscope.

4.3 Results and Discussion

4.3.1 Experimental Results

Before presenting computational analysis, the experimental findings are reviewed briefly. The experimental data have been reported previously [7] but here I newly processed the data in the form suitable for the comparison with the computational results.

Figure 4-1 shows Raman spectra of PEEK after annealing at various temperatures for two hours. It is noticed that there are two peaks in this low wavenumber region - 97cm^{-1} and 135cm^{-1}, and the intensity of 135cm^{-1} peak increases whereas that of 97 cm^{-1} does not change significantly. Figure 4-2 shows WAXRD patterns (inset) and the peak ratios

of the same samples. There are four distinct peaks (Peak A: 2θ =18.9◦, B 20.7◦, C 22.8 ◦, D 28.8 ◦) and the peak ratio changes by annealing at different temperatures. These features in Raman and WAXRD can be used for the evaluation of crystallinity of PEEK, but the mechanism of the change has not been understood so far. In the following sections, I use computational methods to understand these features.

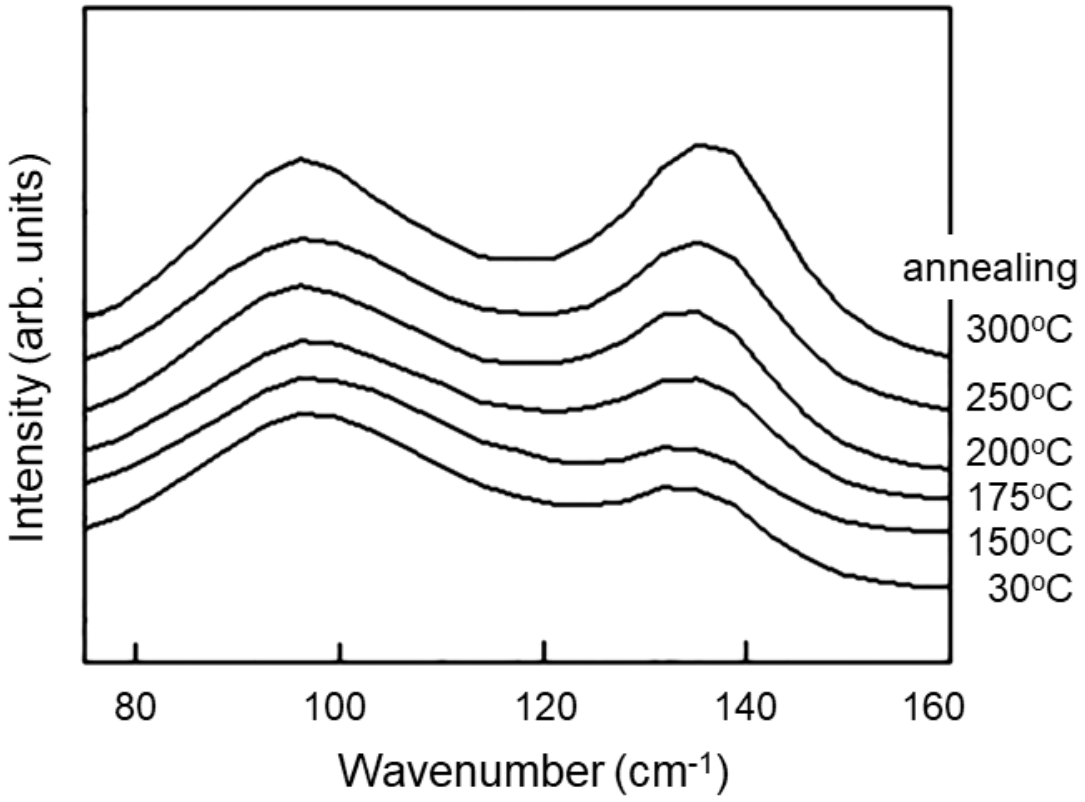

Figure 4-1. Low wavenumber Raman spectra of PEEK films annealed at various temperatures (measurement at room temperature).

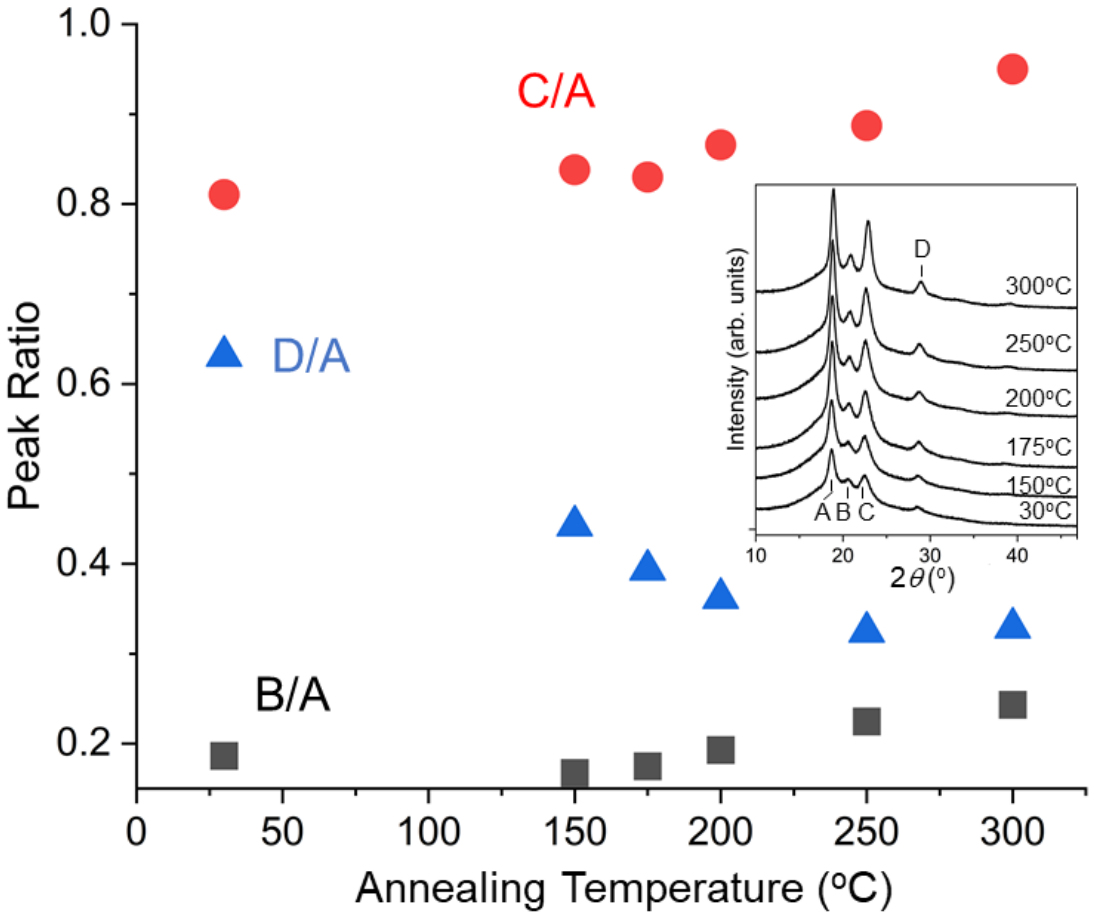

Figure 2. Area ratios of WAXRD peaks B (2θ=20.7◦), C (22.8◦), D (28.8◦) to the peak A (18.9◦) calculated after removing broad background coming from amorphous portion. Inset shows the raw WAXRD spectra.

4.3.2 Calculated Raman spectroscopy of a single molecule PEEK chain

In order to understand the vibration of a PEEK molecule, DFT (b3lyp/6-31G) optimization and calculation of Raman intensity of each vibrational modes of phe-nyl-group-terminated PEEK oligomers with different length were performed using Gaussian 16 package. The result is shown in Figs. 4-3 and 4-4. Figure 4-3 shows Raman spectrum derived from the Raman intensity of each mode with 5 cm^{-1} broadening. The structures

of the molecules are written in the right panel, in which "Ph", "-O-" and "-CO-" denote phenyl group (C6H5-or -C6H4-), ether and ketone, respectively. The peaks around 85-98 cm^{-1} (labeled as "(i)") and 130-145cm^{-1} ("(ii)") are those correspond to the experimental observation (97 cm^{-1} and 135 cm^{-1}). The scaling factor for vibrational analysis using DFT (b3lyp functional) is 0.961 (only ~4% difference) [41] and can be neglected because the shift of the modes due to the chain elongation is larger than 4%.

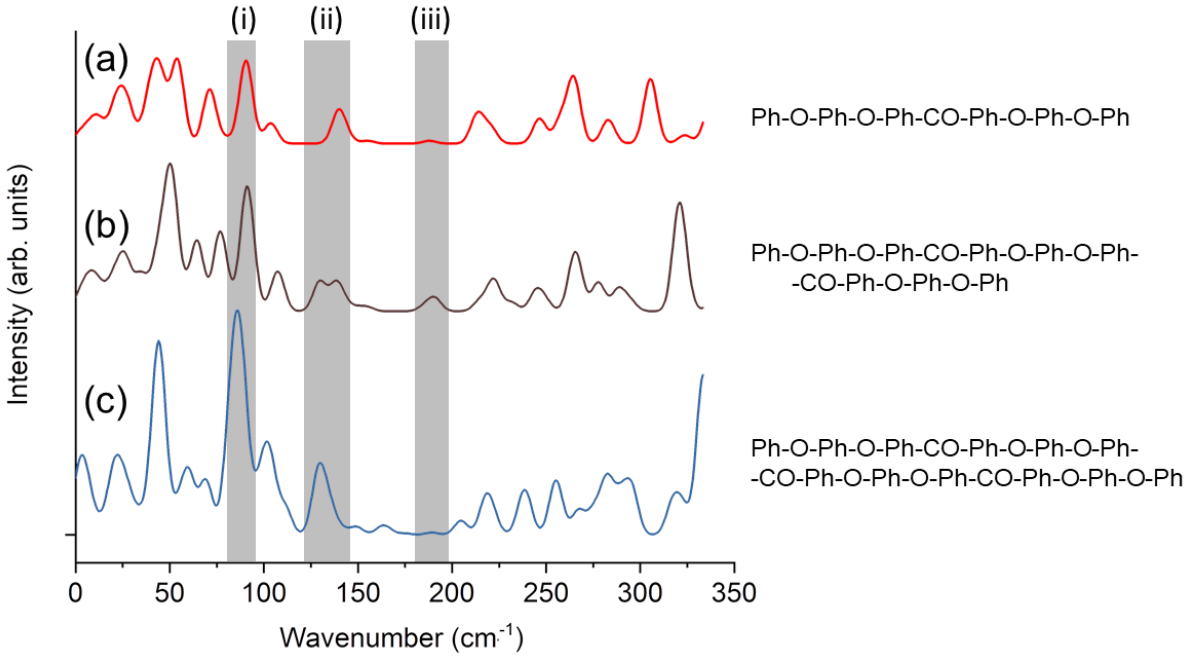

Figure 4-3. DFT-calculated Raman spectra of phenyl-terminated PEEK oligomers shown in the right. Gaussian peaks with 5 cm^{-1} broadening were summed up after multiplying the calculated Raman intensities.

By scrutinizing the atomic motion of each mode (Fig. 4-4), these modes are roughly identified as follows: The 85-98cm^{-1} (mode (i)) is scissoring of ether (Ph-O-Ph) moiety and the 130 ~ 145 cm^{-1} (mode (ii)) is twisting of ketone and connected benzene rings (Ph-

CO-Ph). In Fig. 4-4, the molecule corresponding to Fig. 4-3 (b) is shown. The shorter molecule in Fig. 3(a) has the vibration mode corresponding to Fig. 4-3 (a) and (b) at 90cm^{-1} and 138 cm^{-1}, respectively. For the longer molecule in Fig. 4-3 (c), these modes are split into several modes, i.e. {83, 86, 89 cm^{-1}} and {128,131,135 cm^{-1}} due to the lowered symmetry of the chain after optimization as a single molecule. The Raman active vibration at 190 cm^{-1} appearing as a weak peak(iii) in Fig. 4-3(b), is also displayed in Fig. 4-4(c), because it is observed in the simulation as explained later. This mode is related with the rotation around ketone and becomes lowered (164-189cm^{-1}) when the molecule becomes longer (Fig. 4-3(c))

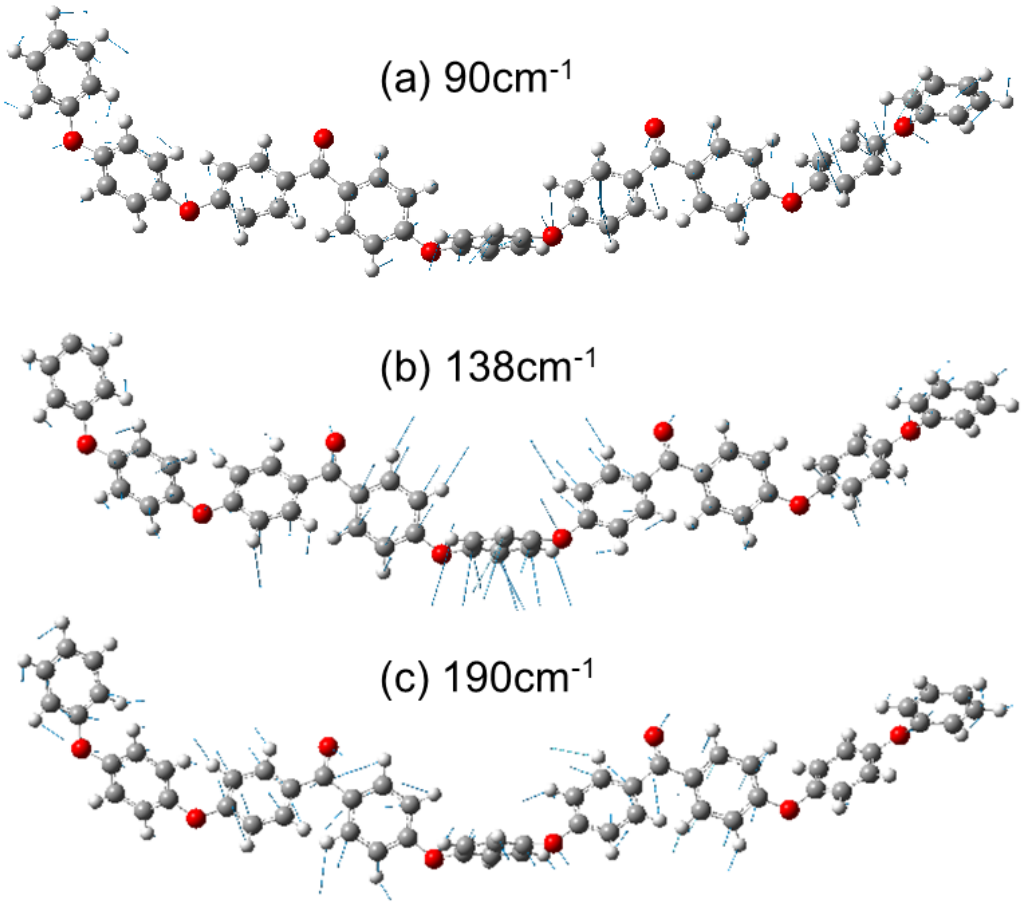

Figure 4-4. Atomic motion in the vibrational modes at (a) 90 cm^{-1}, (b) 138 cm^{-1} and (c) 190 cm^{-1}, calculated for a single oligomer molecule by DFT.

4.3.3 MD simulations

The MD simulation was performed using LAMMPS with GAFF and a 0.1 fs time step. The atomic trajectory was recorded at 5 fs intervals. It is done under NPT constraint, in which the number of particles (N) was constant and the pressure (P) and the temperature (T) were controlled to be certain values with feedback. Following numerical analysis including temporal Fourier transform can be done in several minutes. It is much shorter than vibrational analysis of a polymer system using other techniques. Figure 4-5 shows snapshots from MD trajectory at 300 K and 1 atm.

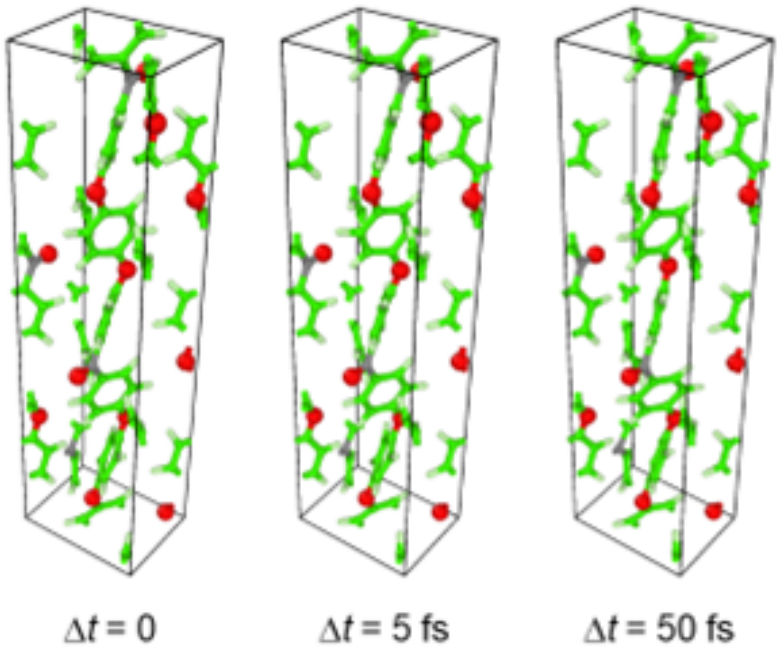

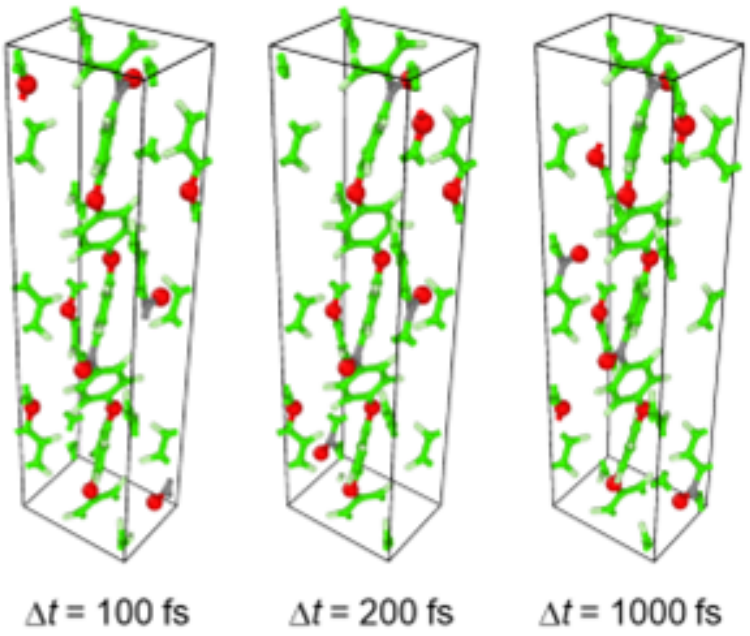

Figure 4-5. Snapshots of MD simulation of a unit cell of PEEK under NPT ensemble at 300 K and 1 atm.

4.3.4 Raman Spectra Simulated from MD

The trajectory of atoms from the MD simulation was used to calculate the local valence electron densities (ρ) at 5 fs interval. The 2 × 3 × 3 × 12 (= 216) points were selected in the unit cell and ρ of each point was calculated as a function of time using Eq. (4). The points are identified using two characters as shown in Fig. 4-6. - circled numbers (1) ~ (18) in ab plane and alphabets A ~ L and M ~ X in c direction.

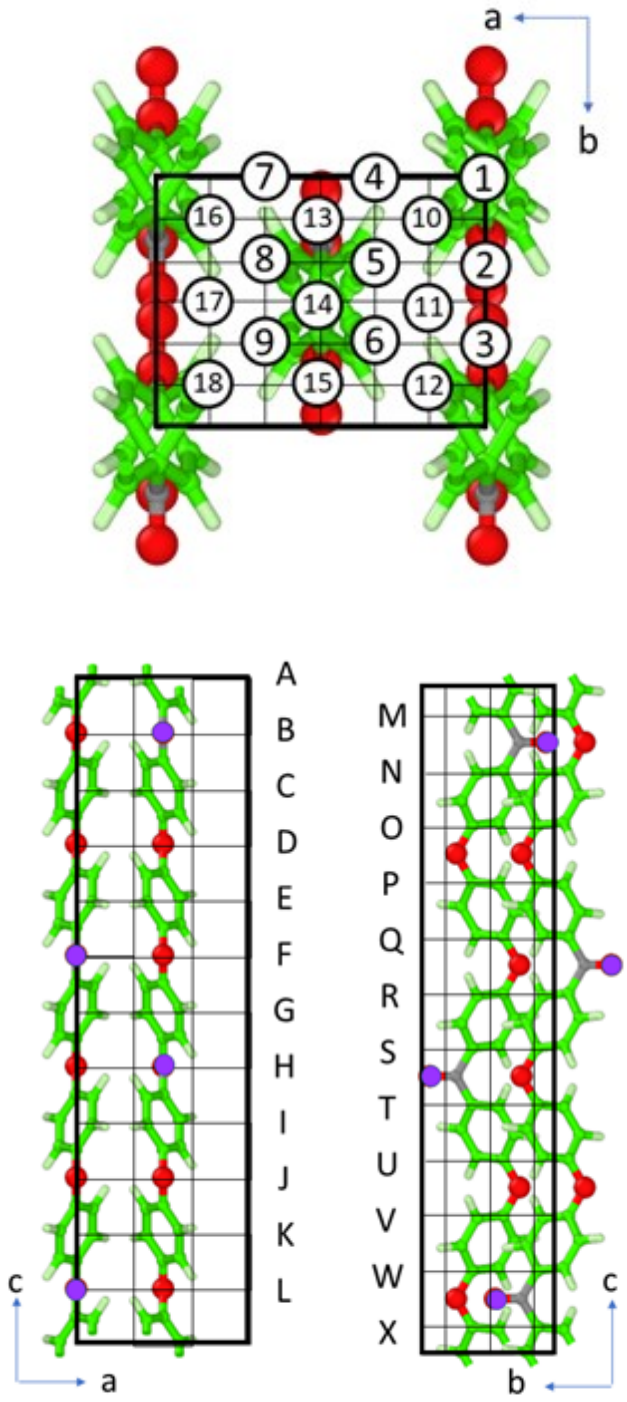

Figure 4-6. Unit cell of PEEK polymer and notation of the calculated points. A point is denoted with a circled number and an alphabet in the figure. Aromatic carbons are green, hydrogens are white, ether oxygens are red, and ketone carbons and oxygens are shown

in purple.

Circled (1)~(9) in the ab plane were coupled with A ~ L in c direction to make 9 × 12 points, and circled (10)~(18) were coupled with M ~ X to make another 9 × 12 points. The local vibrational features were calculated as follows. Approximated "valence electron density" was obtained by Eq. (4) using atomic coordinate snapshot of 300K 1atm NPT simulation recorded at 5 fs intervals. The sum of Eq. (4) at each position (3 × 3 × 12 (=108) positions (①A ~ ⑨L)) was taken over the atoms in the same unit cell and nearest-neighboring unit cells (total 3 × 3 × 3 = 27) using a cut-off distance of 10 Å. The time duration of 450 ps after reaching thermal equilibrium was used for the calculation. The approximated "valence electron density" had 3 × 3 × 12 array data with 9000 points. They were Fourier-transformed and the absolute values were smoothed by smoothing-cubic spline. The result is shown in Fig. 4-7 after converting the frequency axis to the wavenumber unit using Eq. (5). The scaling factor for the vibration frequency derived from the MD using GAFF is reported to be 1.0 [41] and there is no need for scaling the frequency.

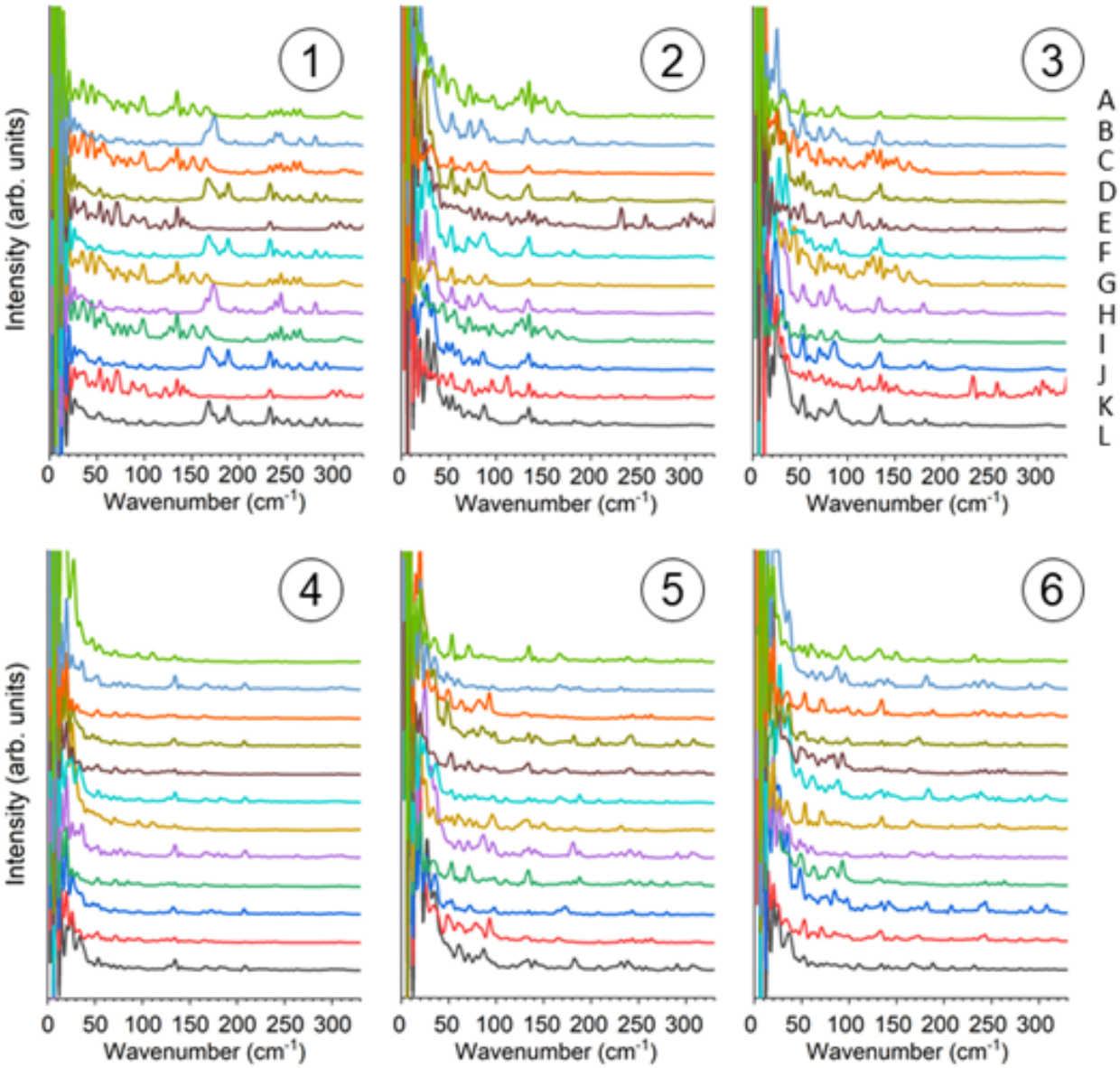
1
2
3
4
5
6
Intensity (arb. units)
Intensity (arb. units)
0 50 100 150 200 250 300
Wavenumber (cm-1)
A
B
C
D
E
F
G
H
I
J
K
L

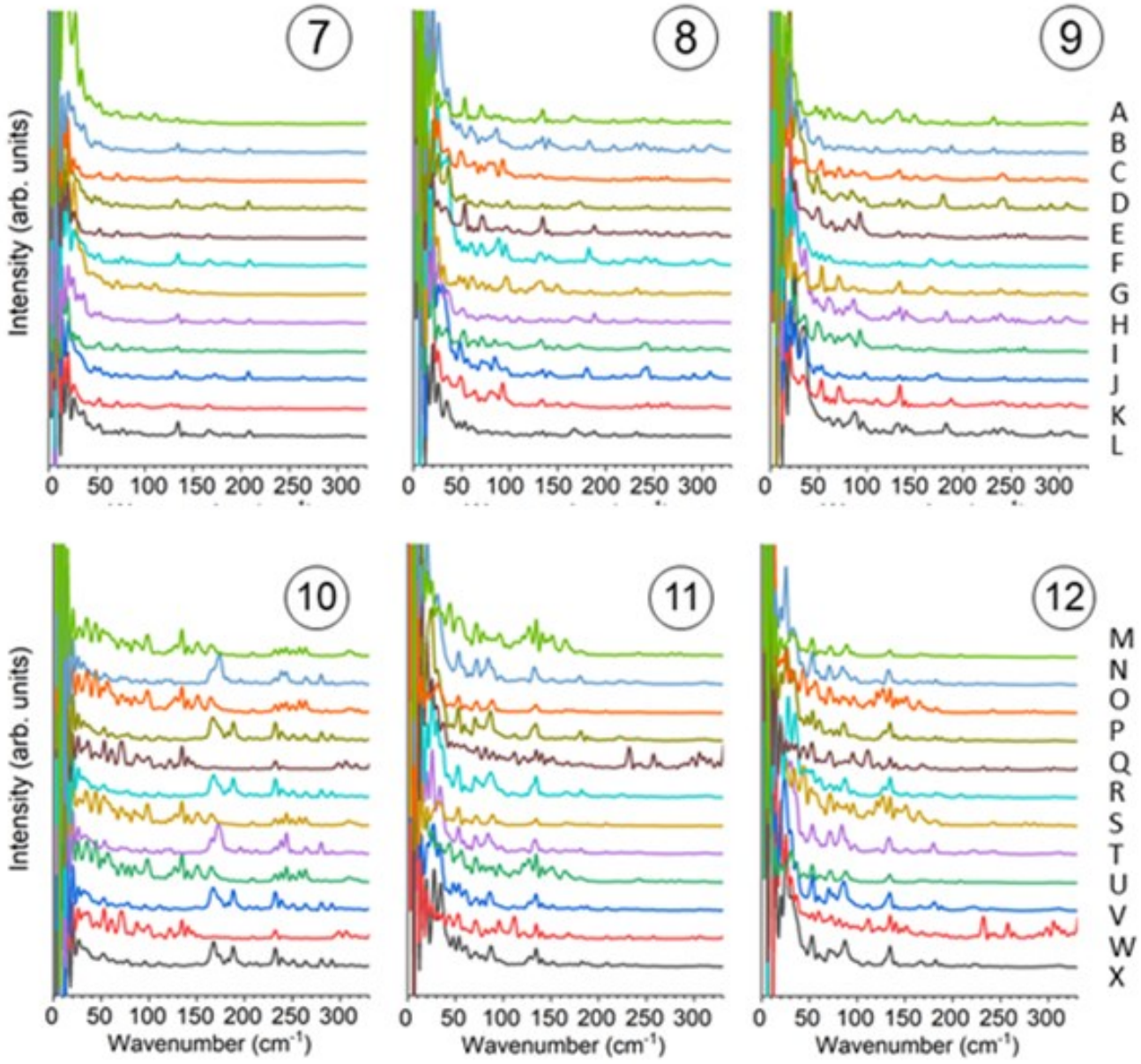
7
8
9
10
11
12
Intensity (arb. units)
Intensity (arb. units)
0 50 100 150 200 250 300
Wavenumber (cm-1)
A B C D E F G H I J K L
M N O P Q R S T U V W X

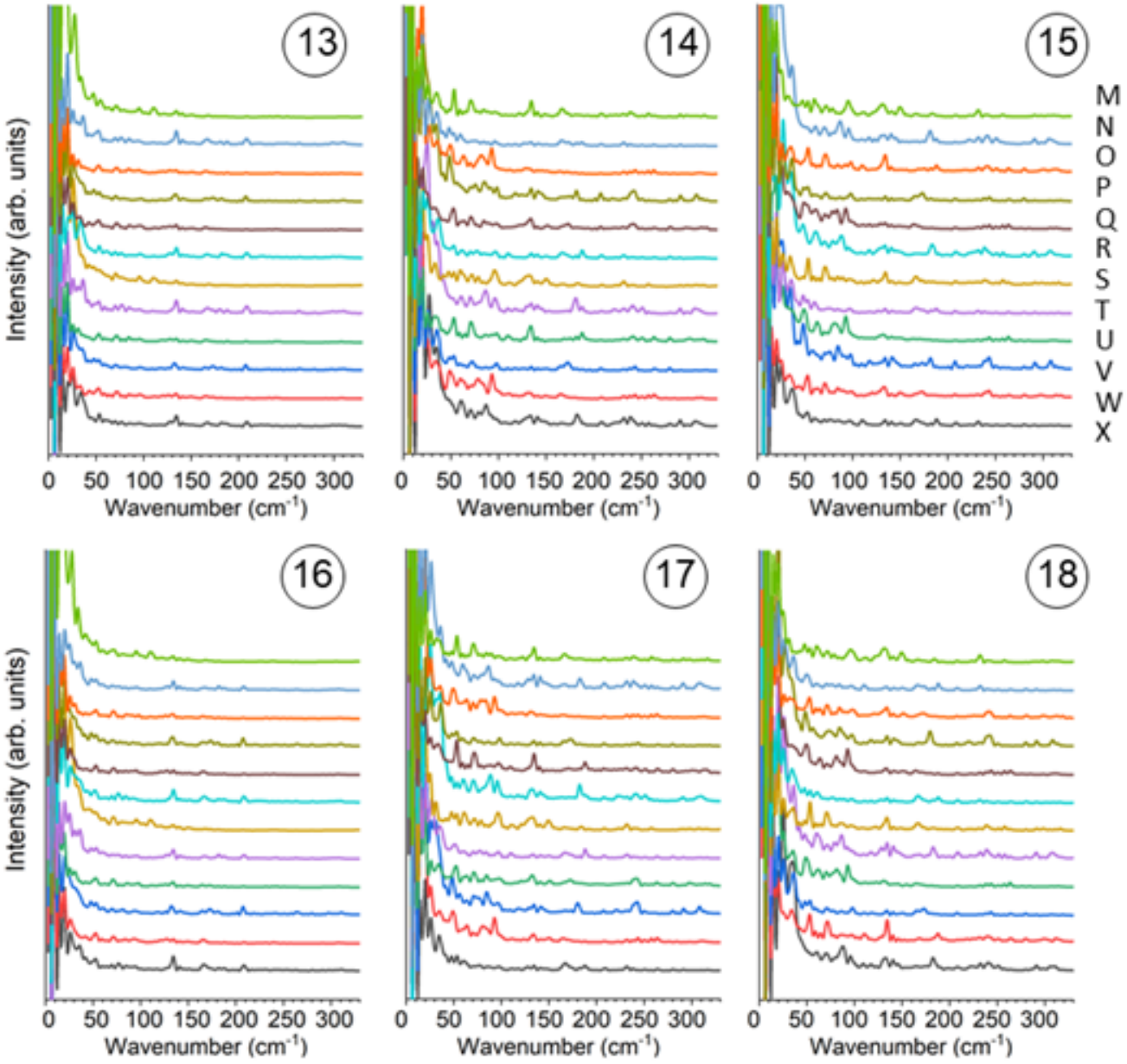
13
14
15
16
17
18
Intensity (arb. units)
0 50 100 150 200 250 300
Wavenumber (cm-1)
M
N
O
P
Q
R
S
T
U
V
W
X

Figure 4-7. Simulated "Raman spectra" of PEEK obtained from Fourier transform of approximate local valence electron density calculated from atomic trajectory in MD.

I notice that several prominent peaks are observed in the low frequency region in Fig. 4-7. Typical ones are picked up and magnified in Fig. 4-8. It is noted that 175 cm^{-1} is very local in some positions in column ① (Fig. 4-8 top left), which coincides with the positions of ketone moiety. Column ⑭ which is located at the center of the molecular chain also shows 175 cm^{-1} peaks. 90cm^{-1} (Fig. 4-8 left) and 135cm^{-1} (Fig. 4-8 right) vibrations are observed more often at the intermolecular spaces (⑤⑨③⑧⑫). than center of the molecular chain (①⑭).

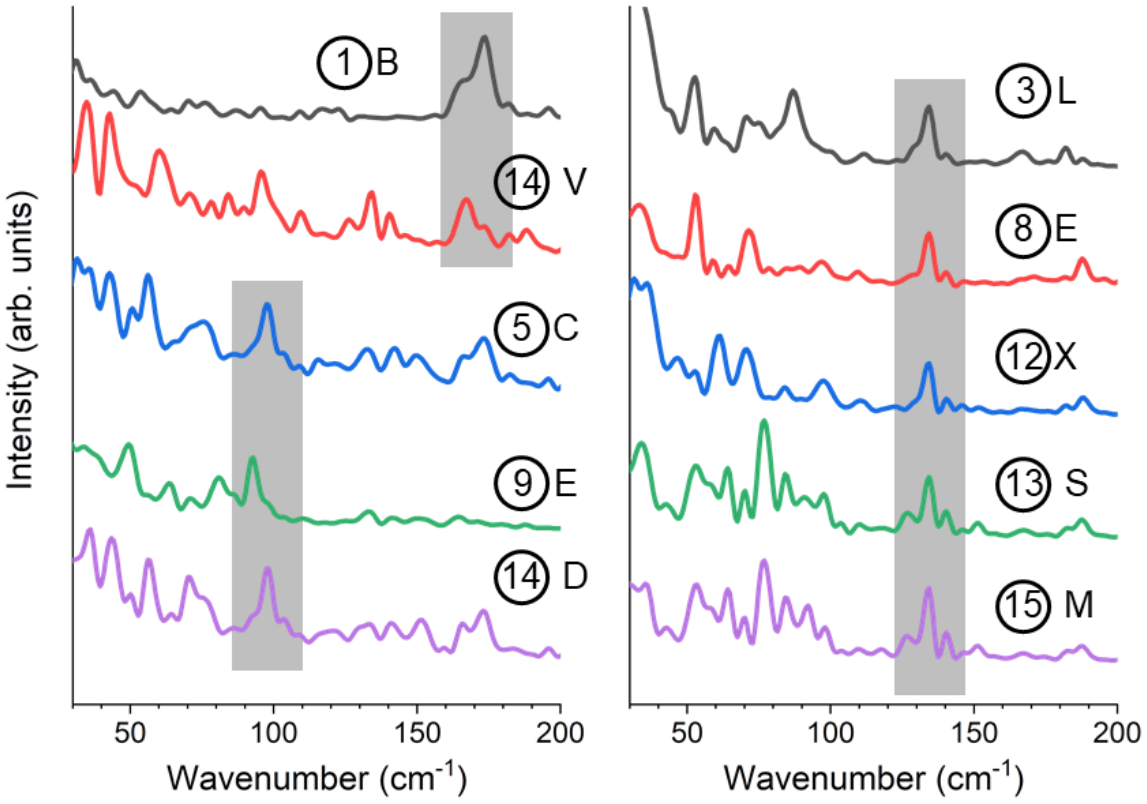

Figure 4-8. Simulated spectra showing characteristic peaks selected from Fig. 4-7.

175cm^{-1} and 90cm^{-1} peaks are hatched in gray in the left panel, and 135cm^{-1} peaks are hatched in the right panel. Circled numbers and alphabets show the point of calculation.

The result presented here shows that Fourier transform of the "valence electron density" (Eq. 4) reproduces the precise vibrational analysis by DFT and the experimental observation. Considering that 135 cm^{-1} Raman signal is much weaker than that of 90 cm^{-1} in DFT of single molecules, and the MD combined with Eq.4 gives prominent peaks at 135 cm^{-1} at the intermolecular positions, I can presume that 135 cm-1 mode is strongly affected by intermolecular interaction. This identification is consistent with the different behavior of 90 cm^{-1} and 135 cm^{-1} peaks during the improvement of crystallinity by annealing experiment.

I must admit that there are some insufficient points of the present analysis of Raman spectra --- the 175cm^{-1} peak found in the analysis was not experimentally observed. It may be explained by the selection rule considering the phase factor of the electric field of light. However, the result can be obtained with much less computational resources compared with first-principle techniques that is difficult to apply to the crystalline polymers and composites.

4.3.5 WAXRD pattern from MD simulation

X-ray diffraction calculation is implemented in LAMMPS. I used this feature to explain the experimental results of WAXRD. First, I used large supercells of infinite polymers, but the structure did not change even when the simulation temperature was raised to 1000

K. I consider the periodic boundary condition (PBC) with connected covalent bonding is too strong restriction. Next I tried to remove the PBC and run NPT simulation. The structure soon became amorphous when the temperature was raised beyond 400 K, and the crystallization was not observed even the system was cooled in the scale of tens of ns. This is because the in-silico crystallization requires time beyond ordinary computation in the case of polymer simulation [42]. I therefore prepared crystalline phenyl-terminated oligomers corresponding to 9 × 9 × 5 unit cell and set PBC to the whole supercell to run NPT calculation. Then the WAXRD patterns from the simulation changed according to the temperature. The result is shown in Fig. 4-9. Still the PBC has an influence and the crystalline order is kept beyond the melting point of PEEK. However, the peak intensities diminish when the temperature is raised. I consider this result can be used to study the effect of degree of disorder to the WAXRD.

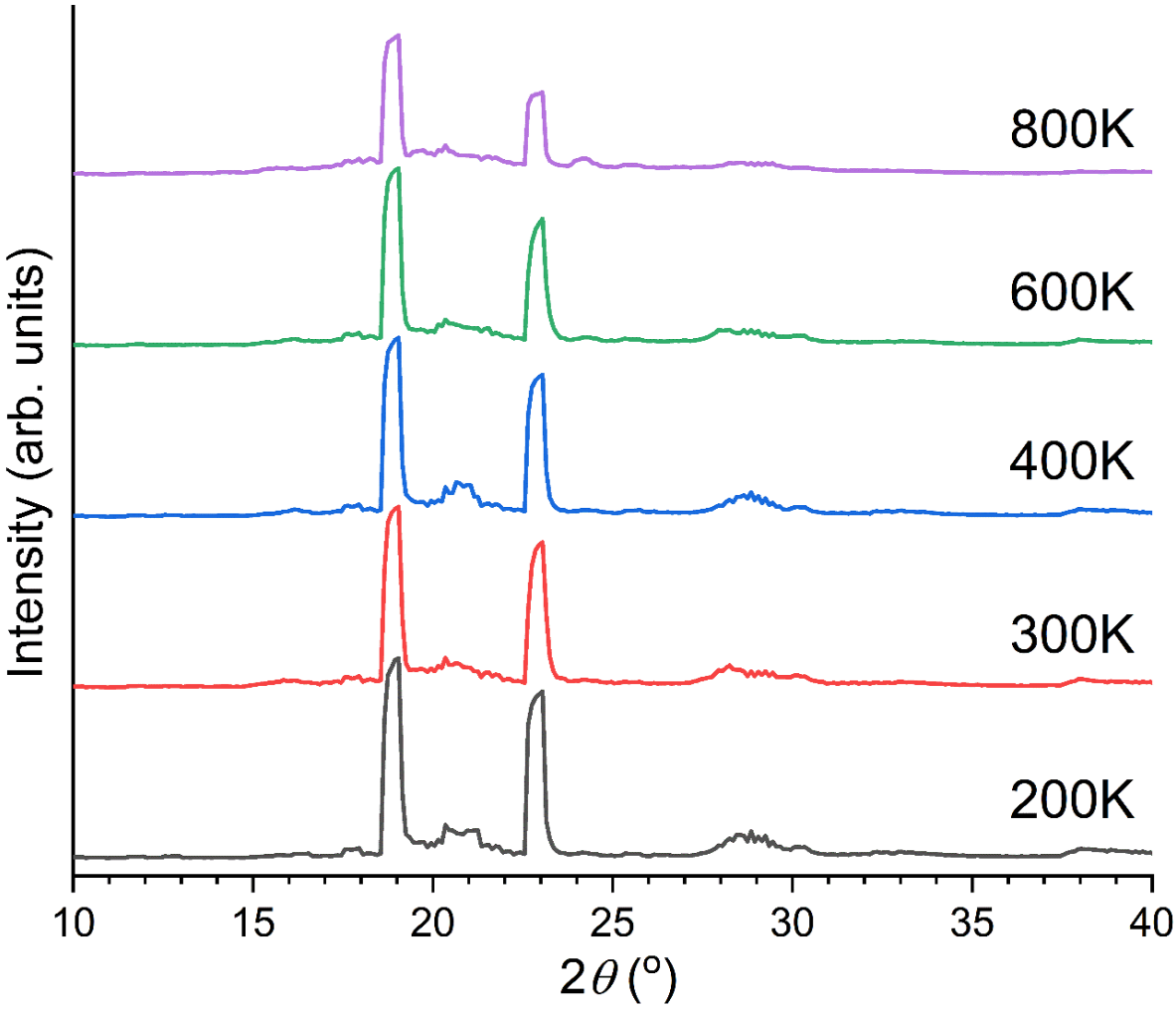

Figure 4-8. WAXRD patterns simulated using LAMMPS for a PEEK oligomer supercell corresponding to 9 × 9 × 5 unit cells.

Since the simulation temperature correspond to thermal disorder in the supercell, it is reasonable to compare the peak area as a function of temperature in the reversed direction as shown in Fig. 4-10. It is noted that peak ratio C/A increases when the crystallinity is increased. This agrees well with the experimental result shown in Fig. 4-2. Peaks A and C correspond to 110 and 200 diffractions, respectively. The result can be explained by considering the order of the nearest neighbor (110) is first established and that of next

nearest neighbor (200) follows to improve when the crystallinity is enhanced during annealing. Peaks B and D correspond to 111 and 211 diffractions. I consider the effect of PBC works strongly in c-direction (the third coordinate) because supercell did not exist in this direction and thus discrepancy with the experiment is observed for these peaks.

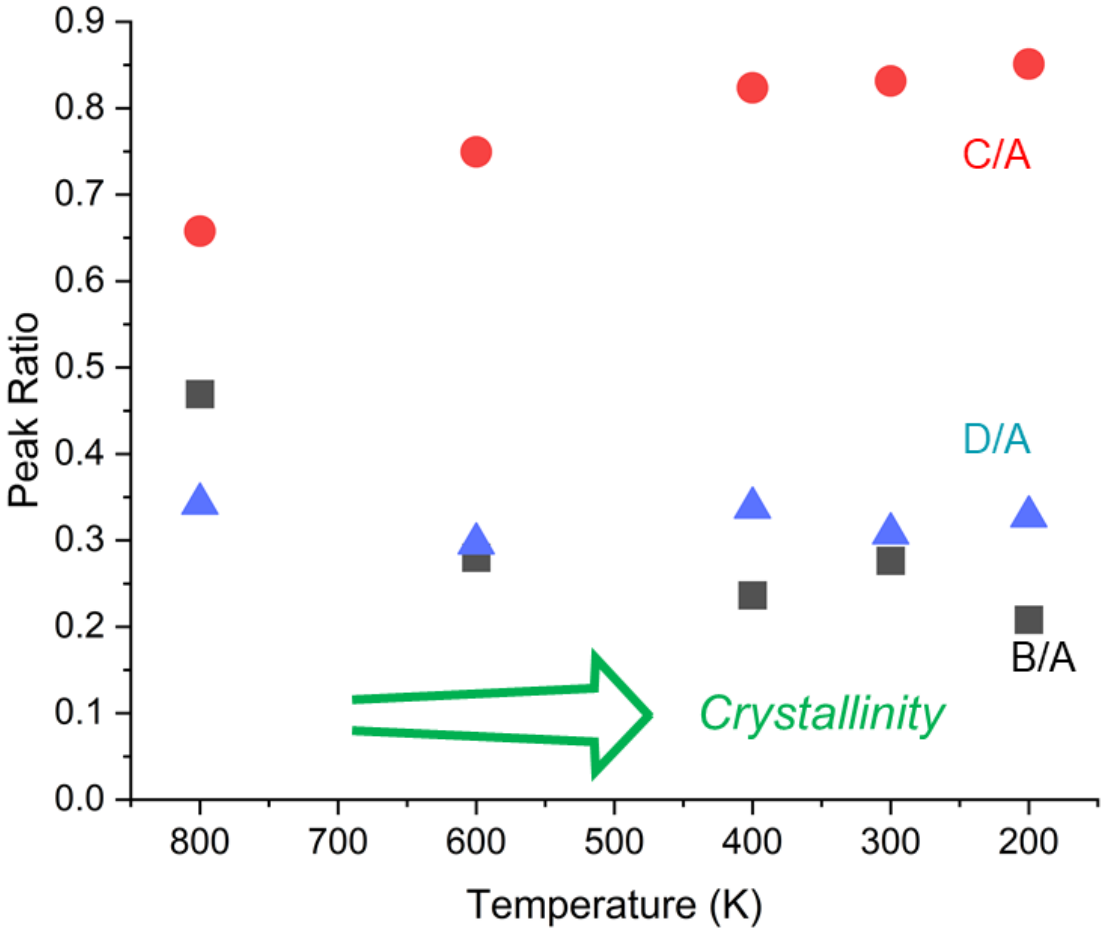

Figure 4-10. Ratio of peak areas as a function of temperatures in the simulation.

4.3.6 Future Improvement of the present method

I have tried to extract the information on the intermolecular vibration using a concept

used in the machine learning of microchemical environment. It is applied to classical MD trajectory of PEEK crystal and it shows agreement with the experiment. However, I admit that estimation of "Raman intensity" of each mode requires more accurate estimation. It is desired to combine the MD with quantum chemical techniques, and some researches in this direction have been reported on quantum MD [43-44]. The reported methods still require much computational resources and cannot be applied to the large systems. For example, use of machine learning techniques to identify the position and direction of Raman-sensitive chemical moieties will be useful for treating the large systems including polymer composites.

4.4 Conclusion

I have proposed and demonstrated new analysis procedure for MD time trajectory to derive approximated Raman spectra in the low frequency region. It involves the local fluctuation of "valence electron density" as a function of time, which is converted to vibrational spectrum by Fourier transform. From the calculation of PEEK polymer, 90 cm^{-1}, 135 cm^{-1}, 175cm^{-1} peaks were observed, among which 90 cm^{-1} and 135 cm^{-1} peaks were experimentally observed. 135 cm^{-1} signal were strongly observed at the inter molecular point, and it is suggested that it is strongly influenced by intermolecular interaction. This explanation agreed well with the experimental behavior of the peak intensity during the crystallization. The WAXRD experiment was compared with the MD with different crystallinity at different temperatures, and nearest neighbor ordering is

more quickly established than that involves next nearest neighbors. Although there is a room for the improvement, the present technique provides a convenient way to estimate vibrational spectra of polymers and their composites with much less demanding computational resources than ordinary techniques.

References:

1. Attwood, T.E.; Dawson, P.C.; Freeman, J.L.; Hoy, L.R.J.; Rose, J.B.; Staniland, P.A. Polymer 1981, 22, 1096–1103.

2. Biron, M. 2nd ed., Elsevier, Amsterdam 2013.

3. Regis, M.; Bellare, A.; Pascolini, T.; Bracco, P. Polym. Degrad. Stab. 2017, 136, 121.

4. Regis, M.; Zanetti, M.; Pressacco, M.; Bracco, P. Mater. Chem. Phys. 2016, 179, 223.

5. Lee, Y.; Porter, R.S. Polym. Eng. Sci. 1986, 25, 633.

6. M, Doumeng.; L, Makhlouf.; F, Berthet.; O, Marsan.; K, Delb.; J, Denape.; F, Chabert. Polymer Testing 2021, 93, 106878.

7. Yamaguchi, M.; Kobayashi, S.; Numata, T.; Kamihara, N.; Shimada, T.; Jikei, M.; Muraoka, M.; Barnsley, J.E.; Fra-ser-Miller, S.J.; Gordon, K.C. Journal of Applied Polymer Science, 2021, 139, e51677.

8. S. L. Hsu, J. Patel, W. Zhao, Chapter 10 - Vibrational Spectroscopy of Polymers. in Molecular Characterization of Polymers: A Fundamental Guide. 2021, p. 369-407.

9. Hitchcock, A.P.; Morina, C.; Zhang, X.; Araki, T.; Dynesa, J.; Stövera, H.; Brash, J.; Lawrence, J.R.; Leppard, G.G. Journal of Electron Spectroscopy and Related Phenomena, 2005, 144–147, 259-269.

10. Mortensen, K.; Talmon, Y. Macromoelcules 1995, 28, 8829-8834.

11. Ellis, G.; Naffakh, M.; Marco, C.; Hendra, P.J. Spectrochim. Acta A 1997, 53, 2279–2294.

12. Louden, J.D. Polym. Commun. (Guildford), 1986, 27, 82–84.

13. Agbenyega, J.K.; Ellis, G.; Hendra, P.J.; Maddams, W.F.; Passingham, C.; Willis, H.A.; Chalmers, J. Spectrochim. Acta A 1990, 46, 197–216.

14. Briscoe, B.J.; Stuart, B.H.; Thomas, P.S.; Williams, D.R. Spectrochim. Acta A 1991, 47, 1299–1303.

15. Stuart, B.H.; Briscoe, B.J. Spectrochim. Acta A 1994, 50, 2005–2009.

16.Lipiäinen, T.; Fraser-Miller, S.J.; Gordon, K.C.; Strachan, C.J. J. Pharm. Biomed. Anal. 2018, 149, 343.

17. Yamamoto, S.; Miyada, M.; Sato, H.; Hoshina, H.; Ozaki, Y. J. Phys. Chem. B 2017, 121, 1128.

18.Yamamoto, S.; Ohnishi, E.; Sato, H.; Hoshina, H.; Ishikawa, D.; Ozaki, Y.J. Phys. Chem. B 2019, 123, 5368.

19. Kramers, H.A.; Heisenberg, Z. Phys. 1925, 31, 681.

20. Dirac, P.A.M. Proc. R. Soc. (London) 1927, 114(767), 710.

21. Hamaguchi, H.; Hirakawa, Nihon Bunko gakkai Tokyo, 1994, 180.

22. Nie, S.; Emery, S.R. Science 1997,275, 1102-1106.

23. Cordero, B.; Gomez, V.; Platero-Prats, A.E.; Reves, M.; Echeverria, J.; Cremades, E.; Barragan, F.; Alvarez, S. Dalton Transactions 2008, 2832-2838.

24. Wen, T.; Altman, R.B. 2017, 18, 302.

25. Shroff, R.; Cole, A.W.; Diaz, D.J.; Morrow, B.R.; Donnell, I.; Annapareddy, A.; Gollihar, J.; Ellington, A.D.; Thyer, R. ACS Synth Biol. 2020, 9, 2927-2935.

26. Gaussian 16, https://www.gaussian.com

27. Thompson, A.P.; Aktulga, H.M.; Berger, R.; Bolintineanu, D.S.; Brown, W.M.; Crozier, P.S.; in 't Veld, P.J.; Kohlmeyer, A.; Moore, S.G.; Nguyen, T.D.; Shan, R.; Stevens, M.J.; Tranchida, J.; Trott, C.; Plimpton, S.J. Comp Phys Comm 2022, 271, 10817.

28. Wang, J.; Wolf, R.M.; Caldwell, J.M.; Kollman, P.A.; Case, D.A. J. Comput. Chem. 2004, 25, 1157-1174.

29. Shimizu, J.; Kikutani, T.; Ookoshi, Y.; Takaku, A. Sen`i Gakkaishi 1985, 41, T461-T467.

30. Jewett, A.I.; Stelter, D.; Lambert, J.; Saladi, S.M.; Roscioni, O.M.; Ricci, M.; Autin, L.; Maritan, M.; Bashusqeh, S.M.; Keyes, T.; Dame, R.T.; Shea, J.-E.; Jensen, G.J.; Goodsell, D.S. "Moltemplate: J. Mol. Biol. 2021, 433, 166841.

31. Dawson, P.C.; Blundell, D.J. Polymer 1980, 21, 577-578.

32. Kumar, S.; Anderson, D.P.; Adams, W.W. Polymer 1986, 27, 329- 336.

33. Hay, J.N.; Langford, J.I.; Lloyd, J.R. Polymer 1989, 30, 489-493.

34. Wakelyn, N.T. J. Polym. Sci. Part C 1987, 25, 25-28.

35. Hay, J.N.; Kemmish, D.J.; Langford, J.I.; Rae, A.I.M. Polym. Commun. 1984, 25, 175-178.

36. Rueda, D.R.; Ania, F.; Richardson, A.; Ward, I.M.; Balta Calleja, F.J. Polym. Commun. 1983, 24, 258-260.

37. Fratini, A.V.; Cross, E.M.; Whitaker, R.B.; Adams, W.W. Polymer 1986, 27, 861-865.

38. Pisani, W.A.; Radue, M.S.; Chinkanjanarot, S.; Bednarcyk, B.A.; Pineda, E.J.; Waters, K.; Pandey, R.; King, J.A.; Odegard, G.M. Polymer 2019, 163, 96-105.

39. Stukowski, A. Simul. Mater. Sci. Eng. 2010, 18, 015012.

40. Momma, K.; Izumi, F. J. Appl. Crystallogr. 2011, 44, 1272-1276.

41. Scott, A.P.; Radom, L. J. Phys. Chem. 1996, 100, 16502-16513.

42. Li, C.; Strachan, A. Polymer 2019, 174, 25-32.

43. Apra, E.; Bhattarai, A.; Baxter, E.; Wang, S.Y.; Johonson, G.E.; Govind, N.; El-Khoury, P.Z. Appl. Spectroscopy 2020, 74, 1350-1357.

44. Carreras, A.; Togo, A.; Tanaka, I. Computer Phys. Commun. 2017, 221, 221-234.

Chapter 5

General Conclusion

In this dissertation, the author had concentrated on both experiment and molecule dynamics methods to study the functional materials, pentacene as an organic functional material was studied through experimental method first, the author had successfully determined the conditions for pentacene crystals growth by naphthalene flux method and fabricated plate-like crystals of pentacene which the sizes about 1 cm. This method can be applied to the crystal growth of other organic semiconductor materials.

C_{60} is another important organic function material. In the experiment of organic semiconductor materials crystal growth, the author found the anomalous phenomenon of heating the mixture of C_{60} and naphthalene. in this part the author combined experimental with molecule dynamics methods to demonstrate the anomalous phenomenon. in the experiment part, the vapor concentration measurement device was established based on the Lambert-beer`s law, the author found that C_{60} will not dissolve in naphthalene but float on the surface of naphthalene as the temperature increases by measuring the concentration of naphthalene vapor of different concentrations of C_{60} and naphthalene samples at various temperatures. The author believes that the reason for this phenomenon may be caused by the change of the C_{60} solid phase during the heating process. The C_{60} and naphthalene mixture model was built and simulations were performed by LAMMPS packages, the output trajectory of the mixture showed that C_{60} molecules will be expelled out from naphthalene molecules. This phenomenon may play an important role in the purification and extraction of C_{60}.

In addition, poly (ether ether ketone) (PEEK) is a polymer functional material which

has a very good corrosion resistance and thermal stability. Low wavenumber Raman spectroscopy and X-ray diffraction are promising techniques for the analysis of crystal ordering but a detailed understanding of the spectra has not been established. The author had investigated PEEK polymers by molecular simulation, and analyzed intermolecular ordering by low-wavenumber Raman spectroscopy and X-ray diffraction. the author found that intermolecular ordering does affect the low wavenumber Raman spectra and the x-ray diffraction as observed in the experiment.

A summary of the important achievements and findings presented in this study as follows:

Chapter 2: the author determined the suitable temperature and concentration for pentacene crystal growth from a naphthalene flux solution, the author successfully established the growth parameter and obtained plate-like crystals of pentacene with almost 1 cm sizes. the author analyzed the crystal structure by x-ray diffraction and found that "bulk type" (interlayer spacing 14.5Å) polymorph crystals was formed. The crystals were made of aligned microtwins.

Chapter 3: the author found an anomalous phenomenon of heating C_{60} and naphthalene mixture and verified through both experimental and simulation methods, while heating the C60 and naphthalene mixture, the C_{60} will be gradually expelled out of naphthalene and floats on its surface, instead of dissolving in it, due to this reason, the vapor of naphthalene will be influenced by the C_{60}, the higher concentration of C_{60}, the more

obvious this inhibitory effect is.

Chapter 4: the author has proposed and demonstrated new analysis procedure for MD time trajectory to derive approximated Raman spectra in the low frequency region. From the calculation of PEEK polymer, 135 cm^{-1} signal were strongly observed at the inter molecular point, and it is suggested that it is strongly influenced by intermolecular interaction. the present technique provides a convenient way to estimate vibrational spectra of polymers and their composites with much less demanding computational resources than ordinary techniques.

Acknowledgements

I would like to express my great gratitude to my supervisor, Prof. T. Shimada who deeply influenced me with his profound academic attainments, rigorous scientific attitude and always enthusiasm. He helped me a lot not only in scientific research, but also in my life.

I also extend my deep respect and sincere thanks to Professors K. Tadanaga, A. Miura, Takashi Yanase, Seiya Yokokura and Taro Nagahama for their valuable discussions and experimental facilities.

Thanks to the members of solid state chemistry laboratory for their kindness and advices.

I would also like to extend my gratitude to my family for their support and understanding.